https://doi.org/10.5194/egusphere-2023-1919
Preprint. Discussion started: 12 September 2023
© Author(s) 2023. CC BY 4.0 License.

Modeling the drivers of fine PM pollution over Central Europe: impacts and contributions of emissions from different sources

Lukáš Bartík[1], Peter Huszár[1], Jan Karlický[1], Ondřej Vlček[2], and Kryštof Eben[3]

[1]Department of Atmospheric Physics, Faculty of Mathematics and Physics, Charles University, Prague, V Holešovičkách 2, 18000 Prague 8, Czech Republic
[2]Czech Hydrometeorological Institute, Na Šabatce 2050/17, 143 06 Prague 4, Czech Republic
[3]Czech Academy of Sciences, Institute of Computer Science (ICS), Pod Vodárenskou věží 271/2, 182 00 Prague 8, Czech Republic

Correspondence: Lukáš Bartík (lukas.bartik@matfyz.cuni.cz)

Abstract. Air pollution nowadays represents the most significant environmental health risk in Europe, with fine particulate matter ($PM_{2.5}$) being among the pollutants with the most critical threat to the human health, especially in urban areas. Identifying and quantifying the sources of $PM_{2.5}$ components are essential prerequisites for designing effective strategies to mitigate this kind of air pollution. In this study, we utilized the numerical weather prediction model WRF (Weather Research and Forecast Model) coupled with the chemistry transport model CAMx (Comprehensive Air quality Model with Extensions) to investigate the relationships between emissions (with a primary focus on emissions covering a wide range of anthropogenic activities) and the concentrations of total $PM_{2.5}$ and its secondary components (ammonium, nitrate, sulfate, and secondary organic aerosol (SOA)) in the region of Central Europe (with a more detailed focus on six large cities in this region, namely Berlin, Munich, Vienna, Prague, Budapest, and Warsaw) during the period 2018–2019 using the PSAT (Particulate Source Apportionment Technology) tool implemented in CAMx and the zero-out method (an extreme case of the brute-force method), which makes this study, taking into account the differentiation of individual GNFR sectors of anthropogenic activity, the only one of its kind for this region.

The use of the PSAT tool showed, among other things, that during the winter seasons, emissions from other stationary combustion (including residential combustion), boundary conditions, road transport, and agriculture–livestock contribute most extensively to the average $PM_{2.5}$ concentrations (their domain-wide average contributions are 3.2, 2.1, 1.4, and 0.9 μgm^{-3}, respectively), while during the summer seasons, the average $PM_{2.5}$ concentrations are mainly contributed by biogenic emissions, followed by emissions from road transport, industrial sources, and boundary conditions (their domain-wide average contributions are 0.57, 0.31, 0.28, and 0.27 μgm^{-3}, respectively). In contrast, the most considerable average seasonal impacts on the concentration of $PM_{2.5}$ when modeling with the SOAP mechanism activated (i.e., with the same SOA formation mechanism that is implemented when using the PSAT tool; we named this sensitivity experiment as the SOAP experiment) are caused by the overall reduction of emissions from other stationary combustion, agriculture–livestock, road transport, and agriculture–other during the winter seasons (their domain-wide averages are 3.4, 2.9, 1.4, and 1.1 μgm^{-3}, respectively), while during the summer seasons, they are induced by emissions from agriculture–livestock, road transport, industrial sources, and other stationary combustion (0.46, 0.45, 0.34, and 0.29 μgm^{-3}, respectively).

https://doi.org/10.5194/egusphere-2023-1919
Preprint. Discussion started: 12 September 2023
© Author(s) 2023. CC BY 4.0 License.

Further, we revealed that the differences between the contributions of emissions from anthropogenic sectors to $PM_{2.5}$ concentration and the impacts of these emissions on $PM_{2.5}$ concentration in the SOAP experiment are predominantly caused by the secondary aerosol components (due to the acting of oxidation–limiting and/or indirect effects). Moreover, the most substantial of these differences, in terms of daily averages in the cities (reaching up to ≈ 15 μgm^{-3} in some of them during winter time) and seasonal averages for the winter and summer seasons (reaching up to 4.5 and 1.25 μgm^{-3}, respectively), are associated with emissions from agriculture–livestock, mainly due to differences in nitrate concentrations.

Finally, we performed one more sensitivity experiment (named the VBS experiment) based on the zero-out method, in which gas-aerosol partitioning and chemical aging of organic aerosol were activated using the 1.5-D VBS scheme, and we also added the estimates of intermediate-volatility and semivolatile organic compounds. We found that their application, in comparison with the results of the SOAP experiment, mainly increases the average seasonal impacts on the concentration of $PM_{2.5}$ caused by the overall reduction of emissions from other stationary combustion and road transport during the winter seasons (the increases reach up to 12 and 4 μgm^{-3}, respectively) and mainly by increasing the average seasonal impact on the concentration of $PM_{2.5}$ produced by the overall reduction of emissions from road transport during the summer seasons (the increase reach up to 2.25 μgm^{-3}).

1 Introduction

Particulate matter (PM) is a component of ambient air pollution that is widely recognized for its harmful effects on human health, including various respiratory and cardiovascular problems that can result in premature death (e.g., Anderson et al., 2012; Apte et al., 2015; Turner et al., 2020). According to the European Environment Agency's latest report on air quality in Europe (EEA, 2022), air pollution is the most significant environmental health risk in Europe, which significantly impacts the health of the European population, particularly in urban areas. Regarding PM with an aerodynamic diameter ≤ 2.5 μm ($PM_{2.5}$, also called fine PM), the report concludes that in 2020, 96 % of the urban population in the European Union was exposed to levels above the health-based guideline level for it set by the World Health Organization (5 μgm^{-3}), which resulted in 238,000 premature deaths.

Although the chemical composition of fine PM (including submicron PM) in Central Europe shows significant spatial and temporal variability, it is generally dominated by organic matter and secondary inorganic aerosols (e.g., Lanz et al., 2010; Putaud et al., 2010; Szigeti et al., 2015; Schwarz et al., 2016; Juda-Rezler et al., 2020; Bressi et al., 2021; Chen et al., 2022). Moreover, Chen et al. (2022) suggested that secondary organic aerosol (SOA) is the main contributor to total submicron PM and dominates organic aerosol across Europe.

In order to design effective strategies to mitigate the adverse effects of PM, it is essential to thoroughly understand the sources of PM, which is still a challenge as PM consists of a host of components with different sources and atmospheric behavior (Hendriks et al., 2013). One of the commonly used ways to source attribution analysis of PM (whose substantial part consists of secondary aerosols) is to use sophisticated chemical transport models (CTMs) such as the Comprehensive Air quality Model with Extensions (CAMx; Ramboll, 2022), the Community Multiscale Air Quality (CMAQ) model (EPA, 2022)

https://doi.org/10.5194/egusphere-2023-1919
Preprint. Discussion started: 12 September 2023
© Author(s) 2023. CC BY 4.0 License.

or CHIMERE (LMD, 2022). It is given by the fact that these models can describe not only the evolution of primary PM but also contains modules that can rigorously control the formation of secondary (in)organic PM from gaseous precursors and its subsequent development, as well as aqueous aerosol chemistry.

Over time, several methods have been developed to study relationships between PM concentrations and emission sources using CTMs. Depending on the approach used for such an analysis of PM sources, they have been generally divided into sensitivity analysis methods and reactive tracer (also called tagged species) methods (e.g., Yarwood et al., 2007; Clappier et al., 2017). The fundamental difference between these two approaches lies in the following: while sensitivity analysis methods estimate the impact on pollutant concentration (in our case, on the total PM or its components) that results from a change of one or more emission sources, reactive tracers methods deal with a source apportionment, which means that they quantify the contribution of an emission source (or precursor) to the concentration of one pollutant (in our case, again, on the total PM or its components) at one given location (Clappier et al., 2017). It is also important to emphasize here that only in the case of linear (or close to linear) relationships between concentration and emissions, impacts (given by sensitivity analysis methods) and contributions (given by reactive tracers methods) are equivalent (or close) concepts (Clappier et al., 2017).

One of the traditional sensitivity analysis methods, frequently used for PM source attribution due to its simplicity and intuitive interpretation, is the zero-out method, which is a special (extreme) case of the brute-force method. As the name suggests, this method quantifies the impact of a particular emission source by comparing the model outputs of a simulation in which emissions from all sources were taken into account (a base simulation) with the outputs of a simulation in which emissions from the source of interest were set to zero (since it seems intuitively obvious that removing a source should reveal the source's impact (Yarwood et al., 2007)). Among the works in which the zero-out method was used to study the impacts of anthropogenic activity sectors on the total concentrations of fine PM in various regions of Europe, we mention the papers of Tagaris et al. (2015), Jiménez-Guerrero (2022), and Arasa et al. (2016) as they differ from most other ones in that their authors used the zero-out method to determine impacts of either all or almost all of anthropogenic activity sectors within the SNAP (Standard Nomenclature for Air Pollution) classification. Concretely, Tagaris et al. (2015) studied these impacts over the whole of Europe but on a model domain with a relatively coarse horizontal resolution (35 km) and only for one month (July 2006). Jiménez-Guerrero (2022) did the same over the Iberian Peninsula using a model domain with a horizontal resolution of 9 km for the summer (June–August 2011) and winter (December 2011–February 2012) scenarios. Finally, Arasa et al. (2016) made such a sensitivity analysis for the region of Madrid and the urban metropolitan area of Madrid on model domains with a horizontal resolution of 3 km and 1 km, respectively, for the year 2010.

Unlike the zero-out method, which can be applied in any CTM, the selection of the tagged species method for PM source apportionment is limited by the selection of the CTM since usually only one such method is implemented in each CTM (if at all). For example, while the CAMx model provides the PSAT (Particulate Source Apportionment Technology; Yarwood et al., 2007) module for this purpose, the TSSA (Tagged Species Source Apportionment; Wang et al., 2009) module can be used in older versions of the CMAQ model, and the ISAM (Integrated Source Apportionment Method; EPA, 2022) module in its newer versions. Tagged species methods have been used in several studies dealing with the origin of fine PM in various regions of Europe: Hendriks et al. (2013) used the LOTOS-EUROS model (Schaap et al., 2008) equipped with a source apportionment

https://doi.org/10.5194/egusphere-2023-1919
Preprint. Discussion started: 12 September 2023
© Author(s) 2023. CC BY 4.0 License.

module based on the PSAT approach (Kranenburg et al., 2013) to establish the origin of ambient PM (PM_{10} and $PM_{2.5}$) over the Netherlands for the years 2007–2009. Skyllakou et al. (2014) used the Particulate Matter Comprehensive Air Quality Model with Extensions (PMCAMx; Fountoukis et al., 2011) together with their extension of the PSAT algorithm (Wagstrom et al., 2008) over Europe on a model domain with a horizontal resolution of 36 km to estimate the impact of local emissions and pollutant transport on primary and secondary fine PM mass concentration levels in Paris for two different periods (a summer period in 2009 and a winter period in 2010). Bove et al. (2014) used CAMx version 5.2 combined with the PSAT module on model domains covering Europe and the area around the city of Genoa (Italy) with a horizontal resolution of 10 km and 1.1 km, respectively, in order to estimate major $PM_{2.5}$ emission sources in the city (and also compare them with the estimates achieved from Positive Matrix Factorisation) during a summer and late autumn period in 2011. Karamchandani et al. (2017) used the PSAT method in CAMx version 6.1 on a model domain with a horizontal resolution of 23 km to identify the main source sectors of fine PM in 16 major European cities (including Berlin (Germany), Warsaw (Poland) and Budapest (Hungary) from the Central European region) for one winter month (February) and one summer month (August) in 2010. Skyllakou et al. (2017) used PMCAMx combined with the extended PSAT algorithm of Skyllakou et al. (2014) over Europe on a model domain with a horizontal resolution of 36 km in order to quantify the sources which contribute to the primary and secondary organic aerosol during three different periods in 2008 and 2009. Pepe et al. (2019) used CAMx version 6.3 together with the PSAT module on model domains covering the Po Valley and the metropolitan area of Milan with a horizontal resolution of 5 km and 1.7 km, respectively, to perform multi-pollutant (including $PM_{2.5}$) source apportionment analyses that combine emission categories and regions for the calendar year of 2010. Coelho et al. (2022) used CAMx version 6.3 together with the PSAT tool to, among other things, quantify the main sources of $PM_{2.5}$ and PM_{10} over four European urban areas (including Sosnowiec (Poland) from the Central European region) for the year 2010. Finally, Pültz et al. (2023) used the LOTOS-EUROS model version 2.1 together with the PSAT algorithm on a European domain with a horizontal resolution of about 28 $\times$ 32 km^2 with a nested domain covering Germany, Poland, and the Czech Republic with a horizontal resolution of about 7 $\times$ 8 km^2 to identify the most relevant sources of PM (namely for $PM_{2.5}$, PM_{10}, and coarse PM) in the Berlin agglomeration area (Germany) covering the period from 2016 to 2018.

In this work, we use an offline coupled modeling framework consisting of a numerical weather prediction model and a CTM on the Central European domain with a moderate horizontal resolution (9 km) to perform: (1) two sensitivity analyses quantifying the impacts of emissions from a wide range of anthropogenic activity sectors on the concentrations of $PM_{2.5}$ and its secondary components (ammonium, nitrate, sulfate, and secondary organic aerosol) using the zero-out method, and (2) source apportionment to estimate the contributions of emissions from the same sectors of anthropogenic activity used in the sensitivity analyses to the concentrations of $PM_{2.5}$ and its secondary components using the PSAT tool, both for the relatively current period covering the years 2018 and 2019. Moreover, in addition to analyzing the outputs determined using both methods over the entire Central European domain, we also focus on six large cities in this region: Prague (Czech Republic), Berlin (Germany), Munich (Germany), Vienna (Austria), Budapest (Hungary), and Warsaw (Poland). Compared to the previous works mentioned above, ours is exceptional in that it is the first to simultaneously implement both approaches (i.e., sensitivity analysis and source apportionment) in one of the regions of Europe.

https://doi.org/10.5194/egusphere-2023-1919
Preprint. Discussion started: 12 September 2023
© Author(s) 2023. CC BY 4.0 License.

2 Methodology

2.1 Models and their configurations used

To describe the regional weather conditions and to drive the chemistry transport model, the Weather Research and Forecast (WRF) Model version 4.2 was adopted in our study. To simulate the chemistry and transport of pollutants, CAMx version 7.10 was used.

The WRF is an atmospheric modeling system designed for research and numerical weather prediction whose detailed description can be found in Skamarock et al. (2019). Our setup handled long- and short-wave radiation transfer using the Rapid Radiative Transfer Model for General Circulation Models (RRTMG; Iacono et al., 2008). Land-surface processes were driven using the Noah land-surface model (Chen and Dudhia, 2001). Urban canopy meteorological effects were invoked by a bulk approach, which treats urban surfaces as any other flat surfaces with physical parameters specific to urban surfaces (like roughness, albedo, etc.). Microphysical processes were parameterized using the scheme proposed by Thompson et al. (2008). Turbulent exchange in the planetary boundary layer (PBL) was solved by the BouLac PBL scheme (Bougeault and Lacarrere, 1989), and convection was calculated using the modified version of the Kain-Fritsch scheme (Kain, 2004).

The CAMx is a state-of-the-science Eulerian chemical transport model, a detailed description of which can be found in Ramboll (2022). To solve the gas-phase chemistry, we applied the CB6r5 mechanism (5th revision of the Carbon Bond mechanism version 6), developed initially as the CB6 by Yarwood et al. (2010), and since then, several times revised (a detailed description of this revisions is presented in Ramboll (2022)). The CB6r5 mechanism consists of 233 reactions among 87 species (62 state gases, 25 radicals) that can also be found in Ramboll (2022). The mechanism was numerically solved using an implementation of the Euler Backward Iterative (EBI) method developed by Hertel et al. (1993).

We used the CF scheme to run aerosol chemistry processes together with the gas-phase chemistry. In this scheme, which divides the aerosol size distribution into two static modes (coarse and fine), primary species can be modeled as fine and/or coarse particles (in our case, both modes were considered). In contrast, all secondary species are modeled as fine particles only. Aqueous aerosol formation in resolved cloud water was driven using the modified version of the RADM (Regional Acid Deposition Model) aqueous chemistry algorithm (Ramboll, 2022), developed initially by Chang et al. (1987). To predict the physical state and composition of inorganic aerosols, we applied the thermodynamic equilibrium model ISORROPIA version 1.7 (Nenes et al., 1998, 1999), which solves partitioning between the gas and aerosol phases for the sodium–ammonium–chloride–sulfate–nitrate–water aerosol system, with an update for calcium nitrate on dust particles.

Two modules can solve organic aerosol-gas partitioning and oxidation chemistry in CAMx version 7.10, and we applied both in the sensitivity analyses (as will be mentioned in more detail later). The first one is the Secondary Organic Aerosol Processor (SOAP) version 2.2, developed initially by Strader et al. (1999) and subsequently updated over time (information about the recent version can be found in Ramboll (2022)). This module: (1) treats primary (directly emitted) organic aerosol (POA) as a single non-volatile species that does not chemically evolve, and (2) considers oxidation of seven gaseous precursors belonging to anthropogenic and biogenic VOCs (volatile organic compounds) to form three semi-volatile (condensable) surrogate compounds for each VOC precursor that can coexist in the gas and aerosol phases based on the pseudo-ideal solution theory

https://doi.org/10.5194/egusphere-2023-1919
Preprint. Discussion started: 12 September 2023
© Author(s) 2023. CC BY 4.0 License.

of Odum et al. (1996). The second module, the 1.5-dimensional (1.5-D) volatility basis set (VBS), represents a hybrid VBS approach that provides a unified framework for gas-aerosol partitioning and chemical aging of both primary and secondary organic aerosol (Koo et al., 2014). It combines the simplicity of the one-dimensional VBS approach proposed by Donahue et al. (2006), in which the evolution of organic aerosol (OA) is described using a set of semi-volatile OA species with volatility equally spaced in a logarithmic scale (the basis set), with the ability to describe the OA evolution in the two-dimensional (2-D) space of oxidation state and volatility used in the (2-D) VBS approach (Donahue et al., 2011, 2012) by using multiple reaction trajectories defined in the 2-D VBS space. Namely, the 1.5-D VBS scheme uses five basis sets to describe varying degrees of oxidation in ambient OA: three for freshly emitted OA (hydrocarbon-like OA from meat cooking and other anthropogenic sources and biomass burning OA) and two for chemically aged oxygenated OA (anthropogenic and biogenic).

As we mentioned in the introduction, for PM source apportionment, it is possible to use the PSAT tool in CAMx, proposed initially by Yarwood et al. (2007). The PSAT modification implemented in the CAMx version we used, a detailed description of which can be found in Ramboll (2022), enables source apportionment of primary PM, ammonium, nitrate, sulfate, SOA, and particulate mercury using a total of 42 tracers for each source region/group. The flexibility of this implementation makes it possible to reduce the number of considered PM species and, thus, also the necessary tracers: in our case, we did not consider the source apportionment of particulate mercury and eight primary elemental species (e.g., iron, manganese or silicon), which can be included by invoking the CF2E scheme. One of the drawbacks of the current implementation of the PSAT tool in the model is that it only describes the OA mass based on the SOAP approach.

To solve the dry deposition of gases and aerosols, we used the methods of Zhang et al. (2003) and Zhang et al. (2001), respectively. Finally, we applied the method of Seinfeld and Pandis (1998) for the calculation of wet deposition.

2.2 Model domains and input data

As mentioned in the introduction, we used an offline coupled model framework of the models described above (i.e., without assuming feedback of air pollutants to processes governing weather conditions) to achieve the goals of this paper. In other words, we first performed a regional weather simulation using the WRF model, the outputs of which we subsequently used to create the required meteorological input fields for all CAMx simulations performed.

The regional weather simulation was conducted on the Central European model domain centered over Prague, Czech Republic (50.075° N, 14.44° E) with a horizontal resolution of 9 $\mathrm{km} \times 9\ \mathrm{km}$ that: (1) contained $208 \times 208 \times 49$ grid boxes in x, y, and z directions, respectively, (2) reached the isobaric level of 50 hPa while the lowermost layer was about 48–50 m thick, and (3) used the Lambert conformal conic map projection. To force this simulation, we used the ERA-interim reanalysis (Simmons et al., 2010). All CAMx simulations were run on one domain, which had the same centering, horizontal resolution, and map projection as the WRF domain but was somewhat smaller compared to it: it consisted of $172 \times 152 \times 20$ grid boxes (the vertical structure was identical to the lowest 20 layers of the WRF domain) and reached approximately 12 km. The model orography of this domain and the analyzed cities' locations are presented in Fig. 1. To create the required meteorological fields for CAMx simulations from the outputs of the weather simulation, we used the WRFCAMx preprocessor. This preprocessor is supplied with the CAMx code (https://www.camx.com/download/support-software/ (last access: 25 January 2023)). One of the

https://doi.org/10.5194/egusphere-2023-1919
Preprint. Discussion started: 12 September 2023
© Author(s) 2023. CC BY 4.0 License.

key parameters the WRFCAMx preprocessor calculates is the vertical eddy-diffusion coefficient that shows to be the dominant driver of urban air pollution (Huszar et al., 2020b, a): in this study, the CMAQ method was applied (Byun and Ching, 1999).

Regarding anthropogenic emissions, we used three different emission inventories: (1) For the areas on the CAMx domain outside the Czech Republic, we applied the emissions from the CAMS (Copernicus Atmosphere Monitoring Service) European anthropogenic emissions - Air Pollutants inventory version 4.2 (Kuenen et al., 2021) for the year 2018. (2) For the area on the domain covering the Czech Republic, we adopted the high-resolution emissions from the Register of Emissions and Air Pollution Sources (REZZO – Registr emisí a zdrojů znečištění ovzduší) for the year 2018 issued by the Czech Hydrometeorological Institute (https://www.chmi.cz, last access: 25 January 2023) together with the emissions from the ATEM Traffic Emissions dataset for the year 2016 provided by ATEM (Ateliér ekologických modelů – Studio of Ecological Models; https://www.atem.cz, last access: 25 January 2023). These inventories provide annual emission totals of carbon monoxide (CO), sulfur dioxide (SO_2), nitrogen oxides (NO_x), ammonia (NH_3), methane (CH_4), non-methane VOCs (NMVOCs), and particulate matter ($PM_{2.5}$ and PM_{10}) aggregated to 12 GNFR (Gridded Nomenclature For Reporting) sectors of anthropogenic activity that are summarized in Table 1. To prepare the data from the mentioned emission inventories to emission files readable by CAMx, including preprocessing of the raw input files, the spatial redistribution of the annual emission totals into the grid of the CAMx domain, chemical speciation, and time disaggregation from annual to hourly emissions, we used the FUME (Flexible Universal Processor for Modeling Emissions) emission model (http://fume-ep.org/, last access: 25 January 2023; Benešová et al., 2018). While for chemical speciation, we used the speciation factors from Passant (2002), for time disaggregation, we applied sector-specific time disaggregation profiles proposed by Denier van der Gon et al. (2011).

Emissions of biogenic volatile organic compounds (BVOCs) were calculated using the Model of Emissions of Gases and Aerosols from Nature (MEGAN) version 2.1 (Guenther et al., 2012) driven by the weather conditions obtained from the regional weather simulation. Vegetation characteristics needed for this model simulation (plant functional types, emission factors, and leaf-area-index data) were derived based on Sindelarova et al. (2014).

2.2.1 Estimates of I/SVOCs emissions

Because emissions of intermediate-volatility organic compounds (IVOCs) and semivolatile organic compounds (SVOCs), which are considered to be important precursors of secondary OA (SOA), are generally missing in current emission inventories, it is common for CTM modeling purposes to estimate them in the form of surrogate species based on sector-specific (alternatively on non-sector-specific) parameterizations (e.g., Giani et al., 2019; Jiang et al., 2019b, 2021). With the intention of including these emissions in our model experiments, we proceeded analogously.

Specifically, to estimate IVOCs and SVOCs emissions produced by gasoline and diesel vehicles, we adopted the methodology used by Giani et al. (2019). Thus, we first estimated IVOCs emissions for gasoline (diesel) vehicles as 0.0397 (1.2748) times their corresponding NMVOCs emissions. Next, we estimated emissions of organic matter in the semivolatile range (OM_{SV}) based on the estimates of IVOCs emissions and using knowledge of the ratio (R) of IVOCs emissions to OM_{SV} emissions (R = 4.62 for gasoline vehicles and R = 2.54 for diesel vehicles) derived from the volatility distribution for gasoline and

https://doi.org/10.5194/egusphere-2023-1919
Preprint. Discussion started: 12 September 2023
© Author(s) 2023. CC BY 4.0 License.

diesel vehicles provided by Zhao et al. (2015) and Zhao et al. (2016), respectively. Furthermore, we used these distributions to redistribute OM_{SV} of both sources into the volatility bins used in the 1.5-D VBS scheme.

Following the methodology justified by Ciarelli et al. (2017) and also used by Jiang et al. (2019b, 2021), we estimated IVOCs emissions from biomass burning as 4.5 times POA emissions summed up from GNFR sectors C (in the territory of the Czech Republic, where we used more detailed data on residential combustion, we applied this parameterization only to the part of POA produced by wood combustion) and L. The IVOCs emissions from other anthropogenic sources we calculated as 1.5 times their corresponding POA emissions, as Robinson et al. (2007) proposed. Finally, to offset the influence of missing SVOCs emissions from biomass burning and other anthropogenic sources besides gasoline and diesel vehicles, we adopted the routinely used approach of multiplying their corresponding POA emissions by a factor of 3 (e.g., Jiang et al., 2019b, 2021).

For the sake of completeness, we add that for CAMx simulations using the SOAP module, we considered only IVOCs estimates (since POA is considered non-volatile in this case), while for those implemented using the 1.5-D VBS scheme, we naturally considered both IVOCs and SVOCs estimates.

2.3 Model experiments: design, validation, and evaluation

Since our main objective is to assess the impacts and contributions of emissions from the broadest possible range of anthropogenic activity on fine PM as well as its secondary components, and we use emission inventories that classify anthropogenic activity into 12 GNFR sectors A–L, we decided to design the model experiments to evaluate all 12 sectors separately. Another aspect we took into account is the dual implementation of the organic aerosol chemistry/partitioning we mentioned earlier. Intending to assess the influence of these different mechanisms on the sector's impacts, we, therefore, implemented two similar sensitivity experiments based on the zero-out method: the first (second), from now on referred to as the SOAP (VBS) experiment, using the SOAP (1.5-D VBS) scheme in all of its CAMx simulations. In order to meet the mentioned experimental design, both sensitivity experiments consist of 13 CAMx simulations: one base (in which emissions from all sources were considered) and 12 perturbed (in each of them, emissions from one of the GNFR sectors A–L were set to zero).

As the PSAT tool is tightly coupled with the SOAP module, we only performed one experiment, from now on referred to as the PSAT experiment, to determine the PM source apportionment. This experiment consists of only one CAMx simulation. In addition to the contributions of the GNFR sectors A–L, it also evaluates the contributions of biogenic emissions and initial and boundary conditions. The basic parameters of all three mentioned experiments are summarized in Table 2.

To demonstrate the capabilities and shortcomings of the model system we used, we compared the modeled concentrations of $PM_{2.5}$ in the studied cities with their measurements stored in the AirBase database (provided by the European Environment Agency (https://discomap.eea.europa.eu/map/fme/AirQualityExport.htm, last access: 25 January 2023)). Naturally, to validate the modeled concentrations, we used only the simulation of the PSAT experiment and the base simulations of the SOAP and VBS experiments since, by the nature of their construction, only these three are different model representations of reality. Taking into account the horizontal resolution used in all these simulations (9 km), we considered it adequate to work only with $PM_{2.5}$ measurements at the background stations. Therefore, we used only hourly (or daily) $PM_{2.5}$ concentration measurements at relevant urban and suburban background stations, which additionally covered at least 75 % of the modeled

https://doi.org/10.5194/egusphere-2023-1919
Preprint. Discussion started: 12 September 2023
© Author(s) 2023. CC BY 4.0 License.

period. As part of the brief validation, we first compared the measured and modeled daily concentrations in the selected cities during the winter (covering December–January–February), spring (March–April–May), summer (June–July–August), and autumn (September–October–November) seasons of 2018–2019 using Pearson correlation coefficient (r), normalized mean bias (NMB), and normalized mean square error (NMSE), the definitions of which are given by Eq. (S1)–(S3) in the Supplement. To be precise, we analyzed their average values while the averaging was performed over all available urban and suburban background stations in the selected city. In addition, we also compared the measured and modeled annual cycles of average monthly $PM_{2.5}$ concentrations (the averaging was performed in the same way as for the statistical indicators).

When evaluating the impacts and contributions, we focused on their average temporal absolute/relative impacts and contributions, the definitions of which are given in Appendix A. More precisely, when assessing the spatial distributions of the impacts and contributions over Central Europe and its surrounding areas, we focused on the average seasonal absolute/relative impacts and contributions, specifically for the winter and summer seasons. In order to provide information about the contributions and impacts of emissions even at a greater temporal resolution, in the case of their evaluation in the selected cities, we focused on the average daily absolute/relative impacts and contributions. In addition, we also determined their seasonal averages in the winter and summer seasons. Before the evaluation, we removed the first 14 days (1–14 January 2018) from all simulations, viewing them as a spin-up time (we also did the same before validating the simulations).

3 Results

3.1 Validation

Table 3 shows the average statistical indicators (r, NMB, and NMSE) comparing the modeled and measured daily $PM_{2.5}$ concentrations during the individual seasons in all studied cities except Warsaw, for which the required station measurements were unavailable. Regarding the correlations, the modeled concentrations in all three simulations correlate best with the measurements during the winter seasons (r = 0.66–0.82) in all studied cities except Vienna, where it occurs in the spring seasons (r = 0.73–0.74). On the contrary, the worst correlated in all three simulations are almost exclusively the concentrations in the summer seasons (r = 0.28–0.55). The average NMB values indicate that the modeled concentrations in all three simulations, excluding those in Prague and Munich during the winter seasons, are, on average, underestimated compared to the measurements. While the most significant underestimations (in terms of the average NMB) occur in the summer seasons (when it ranges from -75.8 to -35.1 %), the smallest deviations between the modeled and measured concentrations (in terms of the absolute value of the average NMB) are most common in the winter seasons. Specifically, the best agreements with the measurements (the average NMB does not exceed ± 10 %) are achieved: (1) in the base simulation of the VBS experiment in Munich during the autumn seasons (-0.4 %) and Budapest during the winter seasons (-3.0 %), (2) in the base simulation of the SOAP experiment in Munich and Prague during the winter seasons (1.5 % and 5.4 %, respectively), and (3) in the simulation of the PSAT experiment in Munich and Prague during the winter seasons (1.6 % and 5.4 %, respectively). The average NMSEs for all three simulations in all the cities are almost always the smallest (NMSE = 21.9–49.7 %) during the winter periods. On the contrary, they are almost always the largest during the summer periods (NMSE = 39.5–274.3 %). At the same time, the average NMSE

https://doi.org/10.5194/egusphere-2023-1919
Preprint. Discussion started: 12 September 2023
© Author(s) 2023. CC BY 4.0 License.

values for the base simulation of the VBS experiment are almost always more or less smaller than those for the other two simulations. Finally, it is essential to point out the striking similarity of all three indicators for the base simulation of the SOAP experiment with those for the simulation of the PSAT experiment in all the cities during all the seasons, which shows (partially proves) the expected high consistency of the model in the prediction of individual PM components during the simulation with and without the use of the PSAT tool.

Figure 2 compares the modeled and measured annual cycles of average monthly $PM_{2.5}$ concentrations in all studied cities except Warsaw (for the above reason). As regards the modeled monthly averages, it is seen that those in the PSAT experiment are almost identical to those in the base simulation of the SOAP experiment in all cities during all months, which again points to the above-mentioned high consistency of the model. At the same time, the modeled monthly averages in both of these simulations are always smaller than their corresponding monthly averages in the base simulation of the VBS experiment: the differences between them are most often up to 2 $\mu g m^{-3}$. The comparison further reveals a certain spatiotemporal conditionality of the model's ability to predict the monthly averages: In Berlin and Vienna, the model underestimates them all year round in all three cases (their average underestimate in the base simulation of the VBS (SOAP) experiment reaches 6.3 (7.2) $\mu g m^{-3}$ in Berlin and 5.0 (6.1) $\mu g m^{-3}$ in Vienna). In Budapest and Prague, the model fails in the same way in capturing the monthly averages during the warm half-year (April–September) and other autumn months in all cases (their average underestimate during this period in the base simulation of the VBS (SOAP) experiment reaches 7.3 (6.2) $\mu g m^{-3}$ in Budapest and 6.5 (5.6) $\mu g m^{-3}$ in Prague); however, in most of the remaining months, it captures them relatively accurately (particularly accurately in Budapest during December and February in the base simulation of the VBS experiment and in Prague from January to March in the base simulation of the SOAP experiment and in the PSAT experiment when the differences between the modeled and measured averages are less than 0.6 $\mu g m^{-3}$). Finally, in Munich, the model underestimates the monthly averages in all three cases from March to August (their average underestimate during this period in the base simulation of the VBS (SOAP) experiment reaches 3.1 (4.3) $\mu g m^{-3}$) but sets them excellently during all autumn (winter) months in the base simulation of the VBS (SOAP) experiment (with differences between the modeled and measured averages up to 0.8 (0.5) $\mu g m^{-3}$).

3.2 Spatial distributions of seasonal $PM_{2.5}$

Before describing the impacts and contributions during the winter and summer seasons, we consider it appropriate to describe the spatial distributions of the modeled seasonal concentrations of $PM_{2.5}$ in the base simulations of the SOAP and VBS experiment during the respective seasons. Because the corresponding distributions in the simulation of the PSAT experiment are almost identical to those in the base simulation of the SOAP experiment, it is not necessary to describe them explicitly.

Figure 3 depicts the above distributions in both base simulations and the difference (VBS - SOAP) between them. In both simulations, the average seasonal $PM_{2.5}$ concentrations in the winter seasons are, except for several areas in the Alps, consistently higher than those in the summer: the domain average (maximum) of their ratio (winter to summer) is 4.2 (9.6) when using the SOAP scheme and 3.7 (9.0) when using the VBS scheme.

In the base simulation of the SOAP experiment, the average concentrations during the winter seasons range from 1 to 35 $\mu g m^{-3}$ (Fig. 3a), with the lowest values (up to 3 $\mu g m^{-3}$) occurring in the highest areas of the Alps. On the contrary,

https://doi.org/10.5194/egusphere-2023-1919
Preprint. Discussion started: 12 September 2023
© Author(s) 2023. CC BY 4.0 License.

among the regions with the most pronounced $PM_{2.5}$ pollution in this simulation during the winter seasons, where its seasonal concentrations exceed 14 μgm^{-3}, are mainly the Po Valley, Italy (on most of its territory, these concentrations exceed 20 μgm^{-3}), most of the territory of the Czech Republic (especially lowland and highly urbanized areas) except for the border mountain areas, some areas in southern and central Poland, some areas in the northern, southern and central parts of the Pannonian Basin, and the area of central Slovenia. The distribution of the average seasonal $PM_{2.5}$ concentrations during the winter seasons in the base simulation of the VBS experiment (Fig. 3c), which range from 1 to 45 μgm^{-3}, is similar in its main features to that in the base simulation of the SOAP experiment. However, they differ quantitatively in that the seasonal concentrations in the base simulation of the VBS experiment are higher in all areas of the domain (Fig. 3e). Moreover, the differences between the average seasonal concentrations of $PM_{2.5}$ during the winter seasons in these two simulations, reaching up to 14 μgm^{-3} in the Po Valley, generally increase when approaching the regions corresponding to the most polluted regions in the base simulation of the SOAP experiment, which we mentioned above.

The average seasonal $PM_{2.5}$ concentrations in the base simulation of the SOAP experiment during the summer seasons reach up to 8 μgm^{-3} but mostly do not exceed 3 μgm^{-3} (Fig. 3b). The lowest values (up to 1 μgm^{-3}) are reached in the Alps and the central region of Slovakia. On the contrary, higher values (in the range of 4–8 μgm^{-3}) are achieved mainly in the Po Valley, in the southern area of the Pannonian Basin, in Silesia, in Prague, and in the southern and western regions of Germany. The corresponding average seasonal concentrations in the base simulation of the VBS experiment reach up to 10 μgm^{-3} but mostly do not exceed 4 μgm^{-3} (Fig. 3d). Compared to the average seasonal concentrations in the base simulation of the SOAP experiment, they are (analogously to the winter seasons) higher in all areas of the domain (Fig. 3f), with the most pronounced differences (exceeding 1 μgm^{-3}) occurring in the regions of the Po Valley, Silesia, and southern, central and western Germany.

3.3 Spatial distributions of impacts and contributions

Here we present the most important results related to the spatial distributions of the average seasonal impacts of emissions on $PM_{2.5}$ concentration (and subsequently also on its secondary components: ammonium (PNH_4), nitrate (PNO_3), sulfate (PSO_4), and SOA) in both sensitivity experiments, as well as those connected with the spatial distributions of the average seasonal contributions of emissions to $PM_{2.5}$ concentration (and its secondary components) in the PSAT experiment. The main differences arising from using both studied concepts are also presented.

3.3.1 $PM_{2.5}$

Figure 4 depicts the spatial distributions of the average seasonal absolute impacts of emissions from individual GNFR sectors on $PM_{2.5}$ concentration during the winter seasons in the SOAP experiment. The corresponding spatial distributions of the average seasonal relative impacts are captured in Fig. S1. The sectors with the highest absolute impacts over the domain (in terms of their averages across the domain) include sector C (other stationary combustion), K (agriculture–livestock), F (road transport), L (agriculture–other), and B (industrial sources) with the average impacts of 3.4, 2.9, 1.4, 1.1, 0.6 μgm^{-3}, respectively. Emissions from other stationary combustion have the most significant average seasonal absolute impact in the areas with the most pronounced $PM_{2.5}$ pollution, in which it mostly exceeds 6 μgm^{-3} (in some localities of the Po Valley,

https://doi.org/10.5194/egusphere-2023-1919
Preprint. Discussion started: 12 September 2023
© Author(s) 2023. CC BY 4.0 License.

it reaches up to 18 μgm^{-3}), representing 40–60 % of the average seasonal $PM_{2.5}$ concentration in the winter seasons. In the rest of the areas, their impacts are in the range of 1–6 μgm^{-3} (except for the highest areas of the Alps, where they are generally below 1 μgm^{-3}), while the areas with the impacts between 4–6 μgm^{-3} are concentrated mainly in the peripheral areas of the Pannonian Basin and on most of the territory of Poland. Emissions from agriculture–livestock cause the average seasonal absolute impacts of 2–4 μgm^{-3} on most of the territory of the domain (even higher impacts occur mainly in the Po Valley (up to 8 μgm^{-3}), but also, for example, in the central region of Poland (up to 6 μgm^{-3}), the impacts up to 2 μgm^{-3} occur in the region of the Alps and central Slovakia). Therefore, the average seasonal absolute impacts of emissions from this sector dominate most of the territory of Germany, Switzerland, and the mountain areas of Austria, representing 25–50 % of the seasonal $PM_{2.5}$ concentration in these areas during the winter seasons. The average seasonal absolute impacts caused by road transport emissions, except for higher-lying areas of the domain, range between 1–6 μgm^{-3}, and values between 4–6 μgm^{-3} are reached only in the Po Valley's central area and Prague. The corresponding average seasonal relative impacts lie mostly between 10–25 %, with higher values occurring especially in the western half of the domain. The last two sectors whose emissions cause the average seasonal absolute impacts higher than 1 μgm^{-3}, at least in specific domain locations, are sectors B (industrial sources) and G (shipping). In the case of the first of them, this occurs mainly in the areas of southern and central Poland, in the southern areas of the Pannonian Basin, in the Po Valley, and in the areas of western and southern Germany; in the case of the second this occurs only in the central area of northern Germany. The average seasonal absolute impacts caused by emissions from other sectors (including sector G for most of the domain) are either small (mostly up to 0.5 μgm^{-3}) or negligible over most of the domain (sectors D and H).

The spatial distributions of the average seasonal absolute (relative) impacts of emissions from individual GNFR sectors on $PM_{2.5}$ concentration during the winter seasons in the VBS experiment are shown in Fig. S2 (S3). As in the SOAP experiment, the sectors with the highest domain average of the average absolute impacts in this experiment are sectors C, K, F, L, and B (4.2, 2.9, 1.7, 1.1, 0.6 μgm^{-3}, respectively). Figure 5, showing the spatial distributions of the differences between the average seasonal absolute impacts on the concentration of $PM_{2.5}$ in the VBS and SOAP experiments during the winter seasons, demonstrates that the use of the 1.5-D VBS scheme (together with the chosen S/IVOCs parametrizations) is mainly manifested by an increase in the average seasonal impacts of emissions from other stationary combustion (sector C) in the areas with the most significant $PM_{2.5}$ pollution mentioned above: this increase ranges between 1–12 μgm^{-3} in the Po Valley and mostly between 1–4 μgm^{-3} in the rest of these areas. Road transport (sector F) is the only one of the other sectors whose emissions increase the average seasonal impact on the concentration of $PM_{2.5}$ when using the 1.5-D VBS scheme in some larger areas by at least 0.5 μgm^{-3}. These areas include mainly the Po Valley (where the increase reaches up to 4 μgm^{-3}), parts of southern and western Germany, parts of central Hungary, and parts of southern and central Poland. For the remaining sectors, the differences between the average seasonal impacts are either small (in absolute value up to 0.5 μgm^{-3}) or negligible.

The spatial distributions of the average seasonal absolute (relative) contributions of emissions from individual categories (all GNFR sectors, biogenic emissions, initial and boundary conditions) to $PM_{2.5}$ concentration during the winter seasons in the PSAT experiment are illustrated in Fig. 6 (S4). The categories with the highest domain average of the average absolute contributions in the experiment are sector C (other stationary combustion; 3.2 μgm^{-3}), boundary conditions (BC; 2.1 μgm^{-3}),

https://doi.org/10.5194/egusphere-2023-1919
Preprint. Discussion started: 12 September 2023
© Author(s) 2023. CC BY 4.0 License.

sector F (road transport; 1.4 μgm^{-3}), sector K (agriculture–livestock; 0.9 μgm^{-3}), sector B (industrial sources; 0.6 μgm^{-3}), and sector L (agriculture–other; 0.5 μgm^{-3}). The average seasonal contributions of emissions from boundary conditions in the lower-lying (higher-lying) areas of the domain range between 2–3 μgm^{-3} (0.5–2 μgm^{-3}), which represent 7.5–30 % (25–50 %) of the average seasonal concentration of $PM_{2.5}$. Comparison of the above-mentioned averages for sectors C, F, and B with their corresponding domain averages of the average seasonal impacts in the SOAP experiment, indicating their similarity for sector C and equality for sectors F and B, is consistent with the striking similarity between the distributions of the average seasonal absolute contributions (Fig. 6) and the distributions of the average seasonal absolute impacts in the SOAP experiment (Fig. 4) for these sectors. The same comparison for sectors K and L, indicating notable differences in their averages, reflects the difference in their corresponding distributions in the PSAT and SOAP experiments.

To quantify the mentioned similarities (differences) more closely, we plotted the distributions of the difference between the average seasonal impacts of emissions in the SOAP experiment and the average seasonal contributions in the PSAT experiment for the individual sectors in Fig. S5. First, it is seen that the investigated differences are the most pronounced for sector K, wherein in the lower-lying areas of the domain, they range between 1.5–4.5 μgm^{-3} (with the highest values reaching in the central area of the Po Valley), while in the higher-lying areas, they lie between 0.1–1.5 μgm^{-3}. Sector L is the only remaining sector for which, at least in part of the domain, these differences exceed 1 μgm^{-3}: this occurs only in some areas in the eastern half of the domain, where they currently exceed 0.5 μgm^{-3} almost everywhere, while in the western half of the domain, they range between -0.1–1.0 μgm^{-3} (mostly between 0.1–0.5 μgm^{-3}). In the case of sectors C and F, the differences in many western and eastern areas of the northern half of the domain (in the case of sector F also in the northwestern area of the Po Valley) are negative (this is more pronounced in the case of sector F, wherein the Po Valley they reach up to -0.75 μgm^{-3}), while in the rest of the domain, they are positive, usually up to 0.5 μgm^{-3} (in the case of sector C (F), they range between 0.5–1 μgm^{-3} in almost the entire (in eastern) area of the Po Valley). For sector E, the differences in the range of 0.1–0.5 μgm^{-3} occur mainly in the southern, central, and western regions of Germany and in the Po Valley, where they locally reach up to 1 μgm^{-3}. For sectors A, B, G, and I, the differences are either negligible or slightly negative (most often up to -0.25 μgm^{-3}); for sectors D, H, and J, the differences are generally negligible. From the comparison of the distributions of the differences between the average seasonal impacts and contributions during the winter seasons for $PM_{2.5}$ (Fig. S5) with their counterparts constructed for the secondary aerosol (considered as the sum of PNH_4, PNO_3, PSO_4, and SOA; Fig. S6a) it can be seen that the above-described differences for $PM_{2.5}$ are almost exclusively the result of the sum of the contributions formed by the analogical differences for the individual SA components: for all the sectors, the differences between these distributions for $PM_{2.5}$ and those for SA in absolute value do not exceed (with a few exceptions) 0.05 μgm^{-3} (not shown).

The spatial distributions of the average seasonal absolute (relative) impacts of emissions from individual GNFR sectors on $PM_{2.5}$ concentration during the summer seasons in the SOAP experiment are shown in Fig. 7 (S7). The sectors with the highest domain average of the average absolute impacts in this experiment are sectors K, F, B, C, and G (0.46, 0.45, 0.34, 0.29, 0.20 μgm^{-3}, respectively). They are also the only sectors whose emissions cause the average seasonal impacts exceeding 0.5 μgm^{-3} in larger areas of the domain (and even higher than 1.5 μgm^{-3} in its specific smaller locations). In the case of sector K, these areas occur in most of the territory of Germany (in its northwestern part, the average seasonal absolute impacts range

https://doi.org/10.5194/egusphere-2023-1919
Preprint. Discussion started: 12 September 2023
© Author(s) 2023. CC BY 4.0 License.

between 1–2 $\mu g m^{-3}$), in some alpine localities of Switzerland and Austria, further in the areas of the Po Valley (in its central area, the average seasonal absolute impacts also range between 1–2 $\mu g m^{-3}$) and in the areas of central and eastern Poland. In connection with sector F, they are located in the Po Valley (in its central area, the average seasonal absolute impacts range from 1–2 $\mu g m^{-3}$) and on a vast area covering almost all of Germany (except its northeastern territory), northern areas of Switzerland and Austria, western Slovakia, the Czech Republic and the southern and central regions of Poland (in the regions of southern Germany as well as in the regions of the Czech Republic with high road traffic, the average seasonal absolute impacts reach 1–1.5 $\mu g m^{-3}$, while in Prague and its surroundings they reach 1.5–2.5 $\mu g m^{-3}$). In the case of sector B, the areas where the average seasonal absolute impacts exceed 0.5 $\mu g m^{-3}$ occur mainly in western, southern, and eastern Germany, in the Po Valley, in central and southern Poland, in eastern Bohemia, and Serbia. Furthermore, in some regions of southern Poland and Serbia, these impacts reach 2–3 $\mu g m^{-3}$, representing the highest average seasonal absolute impacts during the summer seasons in the SOAP experiment. Concerning sector C, these areas are located in the Pannonian Basin and the Po Valley (in the central areas of the Po Valley, the average seasonal absolute impacts range between 1–2 $\mu g m^{-3}$). With regard to sector G, they are located in the Gulf of Venice and the southern and northwestern regions of Germany (in the coastal areas of northwestern Germany, the average seasonal absolute impacts range between 1–2 $\mu g m^{-3}$). Finally, the average seasonal absolute impacts caused by emissions from other sectors are either negligible over most of the territory of Central Europe (sectors D and H) or range over it mostly between 0.05–0.5 $\mu g m^{-3}$.

The spatial distributions of the average seasonal absolute (relative) impacts of emissions from individual GNFR sectors on $PM_{2.5}$ concentration during the summer seasons in the VBS experiment are illustrated in Fig. S8 (S9). Here, specifically in Fig. 8, we present the spatial distributions of the differences between the average seasonal absolute impacts on the concentration of $PM_{2.5}$ in the VBS and SOAP experiments during the summer seasons. They show that using the 1.5-D VBS scheme (together with the chosen S/IVOCs parametrizations) during the summer seasons is mainly associated with an increase in the average seasonal absolute impacts of emissions from road transport (sector F) in the range of 0.1–2.25 $\mu g m^{-3}$ over the entire domain (the increases exceeding 0.75 $\mu g m^{-3}$ occur in southern Poland, roughly in the southern half of Germany, in the north Switzerland and the Po Valley). In addition, the average seasonal absolute impacts increase by at least 0.25 $\mu g m^{-3}$ only for emissions from sector C, specifically in the central areas of the Po Valley, where they range between 0.25–0.75 $\mu g m^{-3}$. In the remaining cases, the differences are either smaller than 0.25 $\mu g m^{-3}$ (especially for emissions from sectors C, E, G, and J) or negligible.

The spatial distributions of the average seasonal absolute (relative) contributions of emissions from individual categories to $PM_{2.5}$ concentration during the summer seasons in the PSAT experiment are illustrated in Fig. 9 (S10). In this case, the categories with the highest domain average of the average absolute contributions are biogenic emissions (BIO; 0.57 $\mu g m^{-3}$), sector F (0.31 $\mu g m^{-3}$), sector B (0.28 $\mu g m^{-3}$), boundary conditions (0.27 $\mu g m^{-3}$), and sector C (0.25 $\mu g m^{-3}$). Except for the northern, marine, and highest parts of the domain, the average seasonal contributions of biogenic emissions lie most often between 0.5–1.5 $\mu g m^{-3}$ (with the highest values being reached in the northwestern region of the Balkan Peninsula), representing 10–55 % of the seasonal concentration of $PM_{2.5}$. The average seasonal contributions of emissions from boundary conditions reach 0.05–1 $\mu g m^{-3}$ (with a certain gradient in the northwest direction), which makes up 2.5–30 % of the seasonal

https://doi.org/10.5194/egusphere-2023-1919
Preprint. Discussion started: 12 September 2023
© Author(s) 2023. CC BY 4.0 License.

concentration of $PM_{2.5}$ (with the highest values reached in the Alpine regions). The distributions of the average seasonal contributions of emissions from sectors D, E, H, and J to $PM_{2.5}$ concentration practically do not differ from their corresponding distribution of the average seasonal impacts in the SOAP experiment (Fig. S11); in the case of sectors A, B, C, I, and L, the differences between them are usually small, the most common to 0.1–0.2 $\mu g m^{-3}$ (at the same time, the contributions are almost always smaller than the impacts). On the other hand, in connection with sectors G, F, and K, the differences between these distributions are more pronounced (up to 0.5, 0.75, and 1.25 $\mu g m^{-3}$, respectively), especially in the above-mentioned locations, where the average seasonal impacts in the SOAP experiment exceed 0.5 $\mu g m^{-3}$. Finally, the comparison of the distributions of the differences between the average seasonal impacts and contributions during the summer seasons for $PM_{2.5}$ (Fig. S11) with their counterparts for secondary aerosol (Fig. S6b) leads to the same conclusion we mentioned for the winter seasons, namely that these differences for $PM_{2.5}$ are essentially given by the sum of the contributions formed by the analogous differences for the individual secondary aerosol components.

3.3.2 Secondary aerosol species

This subsection first deals with the average seasonal contributions of emissions to the individual components of the secondary aerosol and then their comparison with their corresponding average seasonal impacts of emissions on them. We choose this reverse order here to show, in addition to the seasonal contributions themselves, which of the analyzed emission categories emit the precursor(s) of the given secondary aerosol components, which is directly visible from the seasonal contributions since the PSAT tool is constructed in such a way that each secondary aerosol species is linked only to its direct primary precursor(s), i.e., PNH_4 is linked only to NH_3, PNO_3 to NO_x, PSO_4 to SO_2, and SOA to (I)VOCs (Koo et al., 2009; Burr and Zhang, 2011a). At the same time, because the average seasonal impacts on all the inorganic secondary components in the SOAP experiment are almost identical to their counterparts in the VBS experiment (not shown), only those from the SOAP experiment are presented below.

Figure 10 shows that ammonia emissions from sectors K and L contribute the most to the average seasonal concentration of PNH_4 in both seasons: During the winter seasons, the average seasonal absolute contributions of emissions from sector K in the Po Valley reach up to 3 $\mu g m^{-3}$, while in the rest of the domain up to 0.75–1.25 $\mu g m^{-3}$, which usually represent 4–14 % of the seasonal $PM_{2.5}$ concentration (Fig. S12a); the average seasonal absolute contributions of emissions from sector L usually reach 0.5–1 $\mu g m^{-3}$, and thus most often add up to 1–8 % of the seasonal $PM_{2.5}$ concentration (Fig. S12a). During the summer seasons, the average seasonal absolute contributions of emissions from sector K most often range between 0.05–0.7 $\mu g m^{-3}$ (with values exceeding 0.3 $\mu g m^{-3}$ in southern Germany, in the Po Valley, and especially in the northwestern part of Germany), thus representing 2–16 % of the seasonal $PM_{2.5}$ concentration (Fig. S12b); the average seasonal absolute contributions of emissions from sector L reach values between 0.05–0.2 $\mu g m^{-3}$ roughly in the northern half of the domain, where they represent 2–6 % of the seasonal $PM_{2.5}$ concentration (Fig. S12b). The average seasonal absolute contributions from the other sectors emitting ammonia are usually smaller (especially for sectors B, C, D, F, and J in winter seasons) or negligible.

As for PNO_3, Fig. 11 indicates that during both seasons, NO_x emissions from boundary conditions contribute the most to its average seasonal concentration over the entire domain, except for the areas in the Po Valley (in the summer seasons also

https://doi.org/10.5194/egusphere-2023-1919
Preprint. Discussion started: 12 September 2023
© Author(s) 2023. CC BY 4.0 License.

excluding the area of southern Germany): their average seasonal absolute contributions during the winter seasons reach in the lower-lying (higher-lying) areas of the domain 2–3 μgm^{-3} (0.5–2 μgm^{-3}), which represent 7.5–30 % (25–50 %) of the seasonal $PM_{2.5}$ concentration (Fig. S13a), while during the summer seasons, these contributions mostly range between 0.05–1 μgm^{-3} (with values exceeding 0.4 μgm^{-3} mainly in the northwestern half of Germany), representing 2.5–35 % of the seasonal $PM_{2.5}$ concentration (Fig. S13b). When comparing these results with their counterparts for $PM_{2.5}$, which we mentioned above, it is evident that those specific contributions to $PM_{2.5}$ are formed almost exclusively by PNO_3 during both seasons. Further, NO_x emissions from road transport (sector F), the second largest contributor to the average seasonal PNO_3 concentration over most of the domain in both seasons, are its largest contributor in the central area of the Po Valley during both seasons (3–4 μgm^{-3} (0.4–0.8 μgm^{-3}) during the winter (summer) seasons) and in the area of southern Germany during the summer seasons (up to 0.6 μgm^{-3}). The last sector whose NO_x emissions contribute to the average seasonal PNO_3 concentration during the winter (summer) seasons of more than 1.5 μgm^{-3} (0.2 μgm^{-3}) is sector C (G), namely in the central area of the Po Valley (in northwestern Germany). The remaining sectors emitting NO_x (i.e., sectors A, B, I, J, and L), as well as sectors C and G in cases different from those previously mentioned, contribute to the seasonal PNO_3 concentration less (up to 0.1–0.5 μgm^{-3} (0.1–0.2 μgm^{-3}) in the winter (summer) seasons) or negligible.

Figure 12a reveals that SO_2 emissions from sector C usually contribute the most to the average seasonal concentration of PSO_4 in the winter seasons, especially in the eastern half of the domain, where their average seasonal absolute contributions reach 0.4–1.5 μgm^{-3}, representing 4–12 % of the seasonal $PM_{2.5}$ concentration (Fig. S14a). Industrial sources (sector B), power plants (sector A), and shipping (sector G) are the remaining sectors whose SO_2 emissions in selected domain locations contribute to the average seasonal PSO_4 concentration in the winter seasons between 0.1–0.2 μgm^{-3}. At the same time, as can be seen in Fig. 12b, these are the only three sectors whose SO_2 emissions in the selected locations of the domain (for sectors B and A, they are located mainly in Poland and Germany, while for sector G in the Gulf of Venice and Genoa, Italy) contribute to the average seasonal concentration of PSO_4 in the summer seasons up to 0.3–0.6 μgm^{-3}, representing 6–22 % of the seasonal $PM_{2.5}$ concentration (Fig. S14b).

Regarding SOA, Fig. 13a shows that (I)VOC emissions from sector C contribute on average the most to the average seasonal concentration of SOA in the winter seasons, with their average seasonal absolute contributions reaching up to 0.4 μgm^{-3} in the southeastern quarter of the domain and up to 0.8 μgm^{-3} in the Po Valley, representing 1–3 % of the seasonal $PM_{2.5}$ concentration (Fig. S15a). It is also seen that the average seasonal absolute contributions to SOA concentration from the remaining contributing categories (i.e., from sectors E, F, L, biogenic emissions, and boundary conditions) reach up to 0.1–0.2 μgm^{-3} or are negligible. Further, Fig. 13b reveals that biogenic VOC emissions contribute the most to the average seasonal SOA concentration in the summer seasons: their average seasonal absolute contributions range between 0.2–1.75 μgm^{-3} (with the highest values reached in the northwestern region of the Balkan Peninsula), representing 10–55 % of the seasonal $PM_{2.5}$ concentration (Fig. S15b). Again, when comparing these results with their counterparts for $PM_{2.5}$ mentioned above, it is apparent that those specific contributions to $PM_{2.5}$ during the summer seasons are formed almost exclusively by SOA. Finally, it is also seen that the average seasonal absolute contributions to SOA concentration from the remaining contributing categories (i.e., from sectors C, E, F, I, J, K, L, and boundary conditions) either reach up to 0.1–0.4 μgm^{-3} or are negligible.

https://doi.org/10.5194/egusphere-2023-1919
Preprint. Discussion started: 12 September 2023
© Author(s) 2023. CC BY 4.0 License.

In order to compare the given average seasonal absolute contributions to the individual secondary aerosol components (Figs. 10–13) with the corresponding average seasonal absolute impacts of emissions on them in the SOAP experiment, we depict these impacts on PNH_4, PNO_3, PSO_4 and SOA during both seasons in Figs. 14–17. Overall, their mutual comparisons indicate that: (1) for sectors that directly emit the precursor(s) of the given secondary component, the distributions of the average seasonal absolute contributions and impacts differ more or less from case to case; (2) the average seasonal absolute impacts of emissions on the given secondary component acquire non-zero values (and in some cases relatively high or even the highest) even for sectors that do not directly emit its precursor(s) but do emit other precursors that can influence its concentration through the so-called indirect effects, which we deal with in more detail in the discussion. To be precise here, these effects also apply in case (1) if the respective sectors also emit other precursors that can affect the concentration of the respective secondary component.

More specifically, in the case of this comparison for PNH_4 (Fig. 10 against Fig. 14), it can be seen that for sectors K and L, the average seasonal absolute impacts over the entire domain are always smaller than the average seasonal absolute contributions in both seasons (in the lower areas of the domain for sector K up to 0.5–1.5 μgm^{-3} (0.1–0.5 μgm^{-3}) in the winter (summer) seasons, for sector L usually up to 0.5 μgm^{-3} (0.1 μgm^{-3}) in the winter (summer) seasons). On the other hand, during the winter seasons, mainly for sectors F and C (and to a lesser extent also for sectors A, B, G, and I), the average seasonal absolute impacts are more or less higher than the average seasonal absolute contributions, while the highest differences occur for both sectors in the central area of the Po Valley, where they reach up to 1 μgm^{-3} and 0.7 μgm^{-3}, respectively. The same is true, especially for sectors A, B, F, and G during the summer seasons, when these differences reach up to 0.2 μgm^{-3} for the first two sectors and up to 0.3 μgm^{-3} for the second two sectors.

The analogous comparison for PNO_3 (Fig. 11 against Fig. 15) reveals that the overall highest differences between the average seasonal absolute impacts and contributions during both seasons are associated with emissions from sector K (whose average seasonal absolute contributions to PNO_3 are 0 μgm^{-3} as sector K does not emit NO_x): these differences reach in the winter seasons up to 0.5–6 μgm^{-3} (with lower values, up to 2 μgm^{-3}, reached in the higher-lying locations of the domain and with the highest values, above 3 μgm^{-3}, reached in the areas of the Po Valley), while in the summer seasons up to 0.1–1.25 μgm^{-3} (with the highest values reached in the Po Valley and the northwestern region of Germany). Furthermore, during both seasons, there are also more pronounced differences between them for sector L, reaching up to 1–1.5 μgm^{-3} (0.1–0.25 μgm^{-3}) in the winter (summer) seasons. At the same time, it is seen that these differences for the sectors A, B, C, F, G, and I are usually small (in the range between -0.1–0.5 μgm^{-3} (0.05–0.25 μgm^{-3}) during the winter (summer) seasons) and mostly negative in the winter seasons (except for the most part in the southern half of the domain for sectors C and partly also for sector F) and mostly positive in the summer seasons.

Further, the same type of comparison for PSO_4 (Fig. 12 against Fig. 16) shows that during both seasons, the highest differences between the average seasonal absolute impacts and contributions are again related to emissions from sectors K and L (whose average seasonal absolute contributions to PSO_4 are 0 μgm^{-3} in both cases since none of them emits SO_2): these differences are most pronounced in the eastern half of the domain (in the case of sector K also in some areas of Germany), where they locally reach up to 0.3–0.8 μgm^{-3} (0.2–0.5 μgm^{-3}) in the winter (summer) seasons. In addition, it can be seen

https://doi.org/10.5194/egusphere-2023-1919
Preprint. Discussion started: 12 September 2023
© Author(s) 2023. CC BY 4.0 License.

that for sectors A, B, and C (i.e., for sectors that directly emit SO_2), the average seasonal absolute impacts are smaller than the average seasonal absolute contributions, especially in the regions in the eastern half of the domain (up to 0.25–0.5 μgm^{-3}) during the winter seasons. Concerning the average seasonal absolute impacts of emissions on PSO_4 concentration themselves, it is worth mentioning an interesting case in which the reduction of emissions from transport during the winter seasons (sector F in Fig. 16a) causes an increase in the average seasonal PSO_4 concentration, especially over the territory of Poland, by values that exceed its concentration in the base simulation by up to 0.5 μgm^{-3}.

Next, the analogous comparison for SOA (Fig. 13 against Fig. 17) demonstrates that during both seasons, the differences between the average seasonal absolute impacts and contributions are usually small (maximally up to $\pm$ 0.1 μgm^{-3}), except for sector F, where the average seasonal absolute impacts are lower (higher) than the corresponding average seasonal absolute contributions in the areas of the Po Valley (in scattered areas around the Alps) during winter (summer) seasons up to 0.5 μgm^{-3}. Similarly, it is worth mentioning here another interesting case in which the reduction of emissions from transport during the winter seasons (sector F in Fig. 17) causes an increase in the average seasonal SOA concentration in the Po Valley by values that exceed its concentration in the base simulation by up to 0.5 μgm^{-3}.

Finally, the comparison of the average seasonal absolute impacts of emissions on SOA in the VBS and SOAP experiments (Fig. 18 against Fig. 17) points that the most substantial differences between them occur in the winter seasons for emissions from sectors C and F, while in the summer seasons mainly for emissions from sector F. Specifically, in the case of sector C, these differences in the winter seasons are particularly pronounced in most of the territory of the Czech Republic, in the Pannonian Basin and its surroundings (where they reach up to 0.8–1.5 μgm^{-3}); however, the highest values (up to 3.5 μgm^{-3}) they reach in the Po Valley. In the case of sector F, these differences during the winter seasons are most pronounced in the Po Valley, where the negative impact on SOA (described above) deepens to values up to -2 μgm^{-3}. On the other hand, during the summer seasons, these differences for emissions from sector F reach values up to 1.25 μgm^{-3} in the Po Valley, while in the rest of the domain, they reach values mostly up to 0.5–0.75 μgm^{-3}.

3.4 Impacts and contributions in the selected cities

Finally, in this subsection, we present the results connected with assessing the average daily contributions of emissions to $PM_{2.5}$ concentration in the studied cities and those associated with evaluating the average daily impacts of emissions on $PM_{2.5}$ concentration in them within the framework of both sensitivity experiments. Specifically, we focus on describing the sectors whose emissions cause the highest average daily contributions (impacts) and the highest averages of these contributions (impacts) in the winter and summer seasons.

Figure 19 captures the temporal evolution of the average daily absolute contributions of emissions from all investigated categories to the concentration of $PM_{2.5}$ in the studied cities within the PSAT experiment. It can be seen that the sums of the average daily absolute contributions from all categories (representing average daily $PM_{2.5}$ concentrations) are on average higher or even the highest in the late autumn, winter, and early spring months and, conversely, the lowest in the summer months, which is consistent with the annual cycles of average monthly $PM_{2.5}$ concentrations in the cities described during the validation. The highest average daily $PM_{2.5}$ concentrations were reached in Munich (36.4 μgm^{-3}), Berlin (41.9 μgm^{-3}),

https://doi.org/10.5194/egusphere-2023-1919
Preprint. Discussion started: 12 September 2023
© Author(s) 2023. CC BY 4.0 License.

Vienna (42.2 μgm^{-3}), and Prague (59.1 μgm^{-3}) during episodes of elevated $PM_{2.5}$ levels in February 2018, while in Budapest (55.5 μgm^{-3}) and Warsaw (59.7 μgm^{-3}) during such episodes in December 2018. In contrast, during the summer months, the average daily $PM_{2.5}$ concentrations in Berlin, Budapest, and Vienna (in Munich, Warsaw, and Prague) rarely exceed the value of 5 μgm^{-3} (7.5 μgm^{-3}). As for the highest contributions to the average daily $PM_{2.5}$ concentration, it is seen that they generally occur during episodes of elevated $PM_{2.5}$ levels in all cities, especially in the winter months. Moreover, except for Munich, the maximum contributions are caused by emissions from sector C, while in Berlin, Vienna, Warsaw, Prague, and Budapest reach up to 11, 15, 26, 27.5, and 30 μgm^{-3}, respectively. In Munich, where emissions from sector C can produce the second highest contributions (reaching up to 8.6 μgm^{-3}), the maximum contributions are caused by emissions from sector F (reaching up to 8.9 μgm^{-3}), which in other cities can cause the second highest contributions (in Prague reaching up to 16 μgm^{-3}, while in other cities up to 8–10.5 μgm^{-3}). The third-highest contributions, which exceeds 5 μgm^{-3}, are produced by emissions from sector L in Berlin, Munich, Vienna, and Prague, while in Budapest (Warsaw), they are caused by sector K (B) emissions. Regarding the seasonal averages of the average daily absolute (relative) contributions to $PM_{2.5}$ concentration for the winter seasons, Tables S1–S6 show that: (1) in all cities, the three highest ones are caused by emissions from sectors C and F and boundary conditions (BC); (2) the highest ones are caused by emissions from BC in Berlin and Munich (Berlin: 2.35 μgm^{-3} (26.2 %), Munich: 2.50 μgm^{-3} (26.5 %)), while in other cities, they are generated by emissions from sector C (Vienna: 3.97 μgm^{-3} (30.1 %), Warsaw: 6.74 μgm^{-3} (39.0 %), Budapest: 8.89 μgm^{-3} (50.8 %), Prague: 9.45 μgm^{-3} (48.2 %)). Concerning the similar seasonal averages for the summer seasons, the mentioned tables show that among the three highest are those caused by emissions from sectors B, F, and C or biogenic emissions, depending on the specific city. At the same time, it can be seen that, except for the seasonal average caused by emissions from sector F in Prague (1.58 μgm^{-3} (40.7 %)), they do not exceed the value of 1 μgm^{-3} (30 %).

The temporal evolution of the average daily absolute impacts of emissions from individual GNFR sectors on the concentration of $PM_{2.5}$ in the studied cities within the SOAP experiment is shown in Fig. 20. When comparing it with Fig. 19, it can be seen that the sums of the average daily impacts in each of the cities almost copy the temporal evolution of the sums of the average daily contributions (the Pearson correlation coefficient between them reaches a minimum value of 0.97 in all the cities). The total differences between the average daily impacts from the SOAP experiment and the average daily contributions from the PSAT experiment caused by emissions from all anthropogenic sources (i.e., in the sense of the sum of these differences from all anthropogenic sources), which, with a few exceptions, are positive throughout both years in all cities (Fig. S16), acquire the highest values during the autumn and winter months, when they reach in Vienna, Berlin, Budapest, Warsaw, Prague, and Munich up to 11, 11.4, 12.9, 13.4, 16.3, and 19.5 μgm^{-3}, respectively, whereby the differences between the average daily impacts and contributions of emissions from sector K mainly cause them. Fig. 20 further reveals that the three sectors whose emissions cause the highest daily impacts in Berlin, Munich, and Prague (Budapest, Vienna, and Warsaw) are sectors K, C, and F (C, K, and L). At the same time, the maximum average daily impacts are caused by emissions from sector K in Berlin (where they can reach up to 17.3 μgm^{-3}) and Munich (19.7 μgm^{-3}), while in Vienna (17.2 μgm^{-3}), Warsaw (23 μgm^{-3}), Prague (29.7 μgm^{-3}), and Budapest (30.4 μgm^{-3}), they are produced by emissions from sector C. In connection with the seasonal averages of the average daily absolute (relative) impacts on $PM_{2.5}$ concentration for the winter seasons, Tables S1–S6 reveal

https://doi.org/10.5194/egusphere-2023-1919
Preprint. Discussion started: 12 September 2023
© Author(s) 2023. CC BY 4.0 License.

that: (1) in all cities, the three highest ones are caused by emissions from sectors C, K, and F; (2) the highest ones are caused by emissions from K in Berlin and Munich (Berlin: 3.05 μgm^{-3} (34.1 %), Munich: 3.10 μgm^{-3} (33.4 %)), while in other cities, they are produced by emissions from sector C (Vienna: 4.20 μgm^{-3} (31.8 %), Warsaw: 6.62 μgm^{-3} (39.1 %), Budapest: 9.18 μgm^{-3} (52.7 %), Prague: 9.73 μgm^{-3} (49.6 %)). As regards the seasonal averages of the average daily absolute (relative) impacts for the summer seasons, Tables S1–S6 show that among the three highest are those caused by emissions from sectors B, F, K, and C, depending on the specific city. At the same time, it can be seen that, except for the seasonal average caused by emissions from sector F in Prague (1.81 μgm^{-3} (46.8 %)), they do not exceed the value of 1.1 μgm^{-3} (33 %).

Finally, Fig. 21 depict the temporal evolution of the average daily absolute impacts of emissions from individual GNFR sectors on the concentration of $PM_{2.5}$ in the studied cities within the VBS experiment. When comparing it with Fig. 20, it can be seen that the sums of the average daily impacts from both sensitivity experiments follow nearly the same temporal pattern in each of the cities (the Pearson correlation coefficient between them exceeds a value of 0.99 in all the cities). The total differences between the average daily impacts from the VBS and SOAP experiments produced by emissions from all anthropogenic sources (again, in the sense of the sum of these differences from all anthropogenic sources), which are positive throughout both years in all cities, achieve the highest values during the winter months when they reach in Munich, Berlin, Vienna, Warsaw, Prague, and Budapest up to 5.2, 6.2, 7.1, 11.5, 15.8, and 17.7 μgm^{-3}, respectively, whereby the differences between the average daily impacts of emissions from sector C (in Berlin and Munich as well as from sector F) predominantly cause them (Fig. S17). It can be further seen in Fig. 21 that the three sectors whose emissions cause the highest daily impacts in Berlin, Munich, Budapest, and Prague (Vienna and Warsaw) are sectors K, C, and F (C, K, and L). At the same time, the maximum average daily impacts are caused by emissions from sector K in Berlin (where they can reach up to 17.4 μgm^{-3}) and Munich (19.8 μgm^{-3}), while in Vienna (22.4 μgm^{-3}), Warsaw (29.4 μgm^{-3}), Prague (41.5 μgm^{-3}), and Budapest (45.1 μgm^{-3}) , they are produced by emissions from sector C. Regarding the seasonal averages of the average daily absolute (relative) impacts on $PM_{2.5}$ concentration for the winter seasons, Tables S1–S6 reveals that: (1) in all cities, the three highest ones are caused by emissions from sectors C, K, and F; (2) the highest ones are caused by emissions from K in Berlin and Munich (Berlin: 3.06 μgm^{-3} (31.8 %), Munich: 3.12 μgm^{-3} (30.8 %)), while in other cities, they are produced by emissions from sector C (Vienna: 5.14 μgm^{-3} (34.6 %), Warsaw: 7.83 μgm^{-3} (41.2 %), Budapest: 12.12 μgm^{-3} (56.9 %), Prague: 12.39 μgm^{-3} (54.1 %)). As regards the seasonal averages of the average daily absolute (relative) impacts for the summer seasons, Tables S1–S6 show that among the three highest are those caused by emissions from sectors B, F, K, and C (depending on the specific city) and the highest ones are produced in all cities by emissions from sector F (Budapest: 1.04 μgm^{-3} (27.1 %), Berlin: 1.06 μgm^{-3} (28.1 %), Warsaw: 1.21 μgm^{-3} (28.1 %), Vienna: 1.23 μgm^{-3} (31.4 %), Munich: 2.13 μgm^{-3} (38.5 %), Prague: 2.42 μgm^{-3} (51.5 %)).

4 Discussion and conclusions

In this work, we focused on analyzing activity sources of fine PM and its secondary components (with an emphasis on sources from anthropogenic activity) in the region of Central Europe using two different approaches applied within the framework

https://doi.org/10.5194/egusphere-2023-1919
Preprint. Discussion started: 12 September 2023
© Author(s) 2023. CC BY 4.0 License.

of chemical transport modeling. In the first case, we used an extreme case of the brute-force method (the so-called zero-out method) to determine the impacts of a complete reduction of emissions from individual anthropogenic activities on fine PM and its secondary components. In addition, we tested the impact of the implementation of the organic aerosol chemistry/partitioning, together with the inclusion of I/SVOCs emissions estimates, on the changes in the mentioned impacts. In the second case, we used the PSAT PM source apportionment tool to determine the contributions of emissions from individual anthropogenic activities to fine PM and its secondary components. At the same time, we compared the outcomes (impacts and contributions) resulting from both of these approaches.

We first presented the evaluation between the modeled and measured $PM_{2.5}$ concentrations in the selected large cities of the studied region (Berlin, Munich, Vienna, Budapest, Warsaw, and Prague), which, among other things, confirmed the high consistency of the CAMx model in predicting $PM_{2.5}$ concentrations with and without using the PSAT tool. At the same time, it showed that the use of the 1.5-D VBS scheme together with the estimates of I/SVOCs emissions leads to a slight improvement of the overall model prediction of $PM_{2.5}$ in the studied cities (i.e., taking into account all seasons (months) of the year, even if in some cases they can make it a little worse). This improvement results from the fact that when using the 1.5-D VBS scheme together with I/SVOCs emissions, there is an increase in average $PM_{2.5}$ concentrations compared to those modeled by the SOAP scheme (Figs. 2 and 3; and this is almost exclusively due to the rise in POA and SOA concentration (Fig. S18)), which in both cases are mostly underestimated compared to the measurements. Such an improvement in the model prediction of $PM_{2.5}$ when using the 1.5-D VBS scheme (or its modifications) together with additional I/SVOCs emissions is expected since their implementation typically leads to an improvement in the prediction of organic aerosol (Ciarelli et al., 2017; Giani et al., 2019; Jiang et al., 2019b, 2021). At the same time, however, it is necessary to add that the current implementation of this concept is burdened by several uncertainties (some of them are discussed in detail in the mentioned articles) and therefore requires additional revisions that can further improve the model prediction of organic aerosol (and thus the total fine PM).

In connection with our evaluation, Liaskoni et al. (2023) performed a similar comparison of modeled and measured $PM_{2.5}$ concentrations in the same cities that we studied here but for the period 2007–2016. To model $PM_{2.5}$, they used the same version of the CAMx model on a similar domain with the same horizontal resolution but with slightly different settings (their settings in the simulation without wind-blown dust emissions and realized using the ISORROPIA model mainly correspond to those we used in the base simulation of the SOAP experiment), driving meteorological fields obtained by the WRF model, and older emission inputs. In general, the seasonal correlations and NMBs determined by us are in reasonable qualitative agreement with those presented by them: (1) the seasonal correlations are mostly the highest during winter and the lowest during summer; (2) the modeled concentrations are on average underestimated the most during summer, while the greatest match between the modeled and measured concentrations occurs in the cold half-year (October–March). Further, Huszar et al. (2021) also compared modeled and measured average monthly concentrations of $PM_{2.5}$ in these cities, however, for an earlier period (2015–2016). To model $PM_{2.5}$, they also used the CAMx model (albeit in an older version) on a similar domain in the same horizontal resolution but with a slightly different setting (corresponding again mainly to those we used in the base simulation of the SOAP experiment), different meteorological fields obtained by the WRF model, and older emissions. Despite this, the mutual relations of the annual cycles of the monthly $PM_{2.5}$ concentrations determined by them in most of the studied cities show qualitatively

https://doi.org/10.5194/egusphere-2023-1919
Preprint. Discussion started: 12 September 2023
© Author(s) 2023. CC BY 4.0 License.

similar patterns as in our case. The same applies when comparing analogous cycles in these cities, which were reported by Liaskoni et al. (2023). Based on these mutual similarities, we can assume that the differences between modeled and observed $PM_{2.5}$ concentrations in our base simulations (characterized mainly by underestimated modeled values) could be partly due to a combination of similar uncertainty sources mentioned by Huszar et al. (2021), which include underestimated emission inventory (which is partially consistent with the missing I/SVOCs emissions discussed above) and too strong daytime dilution connected with overestimated vertical turbulence. Other important sources of uncertainty in modeled $PM_{2.5}$ concentrations in some regions of Central Europe could be (1) wind-blown dust emissions, especially in the cold half-year (Liaskoni et al., 2023), and (2) estimates of the emissions of biogenic volatile organic compounds, especially in the warm half-year, as they can significantly affect SOA concentrations (Jiang et al., 2019a).

The crucial conclusion of the model evaluation, i.e., more or less significant underestimation of modeled $PM_{2.5}$ concentrations (with a few exceptions), must be considered when interpreting all results concerning the contributions and impacts of emission sources. Overall, it can be assumed that the average absolute contributions and impacts determined by us are, in most cases, slightly underestimated.

As we already mentioned in the introduction, Pültz et al. (2023) used the LOTOS-EUROS model on a domain with a similar horizontal resolution as we used in our experiments to determine the average annual concentration of $PM_{2.5}$ (10.4 $\mu g m^{-3}$) as well as the average annual contributions of emission sectors (contributions from sector C, sectors A and B, boundary conditions, sectors K and L, sector F, biogenic emissions, and other sectors are 3.2, 2.0, 1.4, 1.3, 1.3, 0.5, and 0.7 $\mu g m^{-3}$, respectively) in Berlin during the period 2016–2018. Considering the relatively small time difference between their and PSAT experiments, we can assume a mutual similarity of their results with the counterparts determined from the PSAT experiment. In order to compare them, we determined these counterparts: the average annual concentration of $PM_{2.5}$ is 6.8 $\mu g m^{-3}$ and the average annual contributions of the emission sectors (listed in the same order as above) are 1.0, 1.1, 1.3, 0.9, 1.1, 0.3, and 1.1 $\mu g m^{-3}$, respectively. Contrary to our assumption, the average annual $PM_{2.5}$ concentration in the PSAT experiment is underestimated by a factor of ≈ 1.53. Moreover, it is evident that this underestimation is mainly caused by underestimating the contribution of emissions from sector C (by a factor of 3.2), followed by underestimating the contribution of emissions from sectors A and B (by a factor of ≈ 1.82). These observed differences could be partially explained by the use of different emission databases for the territory of Germany in both experiments: While we used emissions from the CAMS database, Pültz et al. (2023) applied gridded emissions obtained from the GRETA (Gridding Emission Tool for ArcGIS v1.1; Schneider et al., 2016) system with the exception of emissions for residential wood combustion (RWC), which they replaced with a scientific bottom-up inventory accounting for the semivolatile components of these emissions (Denier van der Gon et al., 2015). Thus, they used the RWC emissions increased compared to those officially reported in the GRETA system by a factor of 2–3, which is naturally reflected in the average annual contribution of emissions from sector C (since the RWC emissions contribute to this sector). Considering that the emissions for RWC reported in the CAMS database also do not consider the presence of semivolatile compounds could partially explain the observed largest underestimation of the annual contribution of emissions from sector C in the PSAT experiment.

https://doi.org/10.5194/egusphere-2023-1919
Preprint. Discussion started: 12 September 2023
© Author(s) 2023. CC BY 4.0 License.

When comparing the total monthly contributions of emissions to $PM_{2.5}$ in Berlin, Budapest, and Warsaw determined for February and August 2010 by Karamchandani et al. (2017), we found that compared to our determined total seasonal contributions to $PM_{2.5}$ in the winter and summer seasons, they are higher by factors of 1.7–3.0 and 3.0–3.9, respectively. The decrease in the total contributions determined by us could be partly explained (apart from the inconsistency of the comparison of the total monthly and seasonal contributions, which can also play a role) by the reduction in anthropogenic emissions over the course of 9 years (Karamchandani et al. (2017) used the TNO-MACC_II emission inventory (Kuenen et al., 2014) for the year 2009). However, differences in other factors, such as the spatial resolution of model experiments, driving meteorological fields, or other emission inputs, should also participate in it. A deeper qualitative comparison between the compositions of the contributions from the individual sectors determined by them and us shows the persistence of the dominance of the contributions from other stationary combustion (sector C), followed by the contributions from road transport (sector F), public power and industry (sectors A and B: since they used different nomenclature of anthropogenic sectors, these two sectors are difficult to distinguish between each other in their work and therefore we consider here the mutual influence of their emissions), and agriculture (sectors K and L) in all three cities during winter. In contrast to our findings, in their case, the contributions of emissions from boundary conditions do not appear among the most significant contributions during winter, while this is the case during summer. The observed discrepancy during winter could partly be explained by the fact that they used a model domain extending over Europe. Thus, the contributions of anthropogenic emissions released from European regions outside our domain are included directly in their determined contributions from individual anthropogenic sectors. The fact that we did not include dust emissions in the PSAT experiment, which Karamchandani et al. (2017), on the other hand, considered in the domain and boundary conditions framework, could somewhat clarify the observed discrepancy between the contributions during summer. Overall, the contributions found by us and them during the summer are less consistent than those during the winter.

Regarding the differences between the contributions and impacts determined for $PM_{2.5}$ during both studied seasons, we have shown that they were generated almost exclusively by secondary aerosol components. This conclusion fully agrees with the results of Koo et al. (2009), who showed excellent agreement between the contributions and impacts determined for primary $PM_{2.5}$. As they argue, this is to be expected because the source–receptor relationships for primary PM are essentially linear and not affected by any indirect effects. The same argumentation can be used in our case as well. Moreover, Koo et al. (2009), as well as Burr and Zhang (2011a, b) (who applied the same methods as we did to determine the contributions and impacts of emissions above the eastern United States for January and July 2002), shed light on the general principles (along with specific examples) explaining the essence of the differences between the two approaches. These differences are caused by the acting of (1) oxidation–limiting effects in the perturbed and base simulation of sensitivity experiments as well as in a simulation with the applied PSAT mechanism and/or (2) indirect effects, which are not considered when using the PSAT mechanism, in the perturbed simulation. The PSAT mechanism, as we have already mentioned and also shown when evaluating the seasonal contributions of secondary aerosol components, assigns contributions to a specific secondary aerosol component (e.g., PNH_4) only to sectors (sources) that emit its direct precursor(s) (i.e., NH_3), and thus considers only direct effects. As an example of an indirect effect (in general, it is an effect in which a change in the concentration of a specific secondary aerosol component is

https://doi.org/10.5194/egusphere-2023-1919
Preprint. Discussion started: 12 September 2023
© Author(s) 2023. CC BY 4.0 License.

conditioned by a modification in the emissions of its indirect gaseous precursor(s)), we mention a decrease in the concentration of PNO_3 caused by a significant reduction in the emissions of NH_3 from agriculture–livestock (sector K, its dominant source), which limits the production of ammonium nitrate (NH_4NO_3), leaving more HNO_3 in the gas phase. This decrease in the concentration of PNO_3 in the perturbed simulation is naturally reflected in the values of the determined seasonal (daily) average impacts of emissions from sector K on PNO_3, which in turn are mainly responsible for the overall highest differences between the seasonal (daily) contributions to $PM_{2.5}$ and their corresponding impacts found among all anthropogenic sectors just for sector K (Figs. S5, S11, and S16). For a more detailed description of other indirect and oxidation–limiting effects, with the help of which it is possible in principle to clarify other observed differences between the contributions and impacts in our work, we refer to the articles mentioned above.

The main conclusions about the contributions (impacts) of emissions to (on) the concentrations of fine PM and its secondary components, established in this paper for the region of Central Europe and the selected large cities, can be briefly summarized as follows:

- In general, the average seasonal/daily absolute/relative contributions (impacts) of emissions to (on) the concentration of $PM_{2.5}$ and its secondary components are strongly spatially and temporally conditioned.

- In the winter seasons, the average seasonal absolute contribution from other stationary combustion dominates most of the region's territory except for its western areas, followed by the average seasonal absolute contributions of emissions from boundary conditions, road transport, agriculture–livestock, industrial sources, and agriculture–other (their domain-wide averages are 3.2, 2.1, 1.4, 0.9, 0.6 and 0.5 μgm^{-3}, respectively). In the summer seasons, the average seasonal absolute contribution from biogenic emissions dominates most of the region's territory, followed by the average seasonal absolute contributions of emissions from road transport, industrial sources, boundary conditions, and other stationary combustion (their domain-wide averages are 0.57, 0.31, 0.28, 0.27, and 0.25 μgm^{-3}, respectively). The highest daily contributions to the average daily $PM_{2.5}$ concentration, occurring during episodes of elevated $PM_{2.5}$ levels in all cities, especially in the winter months, are predominantly produced by emissions from other stationary combustion, followed by emissions road transport. The three highest seasonal averages of the average daily absolute contributions to $PM_{2.5}$ concentration during the winter seasons in all cities are caused by emissions from other stationary combustion, road transport, and boundary conditions (their order depends on the specific city), while during the summer seasons, they are caused by emissions from industrial sources, road transport, other stationary combustion or biogenic emissions, depending on the specific city. The main contributors to the average seasonal concentration of PNH_4 in both seasons are NH_3 emissions from agriculture–livestock, and agriculture–other. NO_x emissions from boundary conditions and road traffic are the main contributors to the average seasonal concentrations of PNO_3 in both seasons. The main contributors to the average seasonal concentration of PSO_4 during the winter seasons are SO_2 emissions from other stationary combustion, power plants, and industrial sources, while during the summer seasons, they are mainly emissions from power plants, industrial sources, and shipping. Finally, the main contributor to the average seasonal concentration of SOA during the winter and summer seasons are (I)VOCs emissions from other stationary combustion and biogenic VOCs emissions, respectively.

https://doi.org/10.5194/egusphere-2023-1919
Preprint. Discussion started: 12 September 2023
© Author(s) 2023. CC BY 4.0 License.

- In contrast, the most enormous average seasonal absolute impacts on $PM_{2.5}$ concentration caused by anthropogenic emissions in the SOAP experiment during the winter seasons are those from other stationary combustion, agriculture–livestock, road transport, agriculture–other, and industrial sources (their domain-wide averages are 3.4, 2.9, 1.4, 1.1, 0.6 μgm^{-3}, respectively), while during the summer seasons, among them are those from agriculture–livestock, road transport, industrial sources, other stationary combustion, and shipping (0.46, 0.45, 0.34, 0.29, 0.20 μgm^{-3}, respectively). Further, the sectors whose emissions cause the highest daily impacts on $PM_{2.5}$ concentration in the cities are primarily other stationary combustion and agriculture–livestock, followed by road transport or agriculture–other, with their specific order depending on the specific city. The three highest seasonal averages of the average daily impacts on $PM_{2.5}$ concentration during the winter seasons in the cities are rendered by emissions from other stationary combustion, agriculture–livestock, and road transport, while among the three highest such averages during the summer seasons are those generated by emissions from industrial sources, road transport, agriculture–livestock, and other stationary combustion, depending on the specific city.

- The differences between the contributions of emissions from anthropogenic sectors to $PM_{2.5}$ concentration in the PSAT experiment and the impacts of these emissions on $PM_{2.5}$ concentration in the SOAP experiment are predominantly induced by the acting of oxidation–limiting and/or indirect effects on secondary aerosol components. The most substantial of these differences, in terms of daily averages in the cities (reaching up to ≈ 15 μgm^{-3} in some of them during winter time) and seasonal averages for both seasons (reaching up to 4.5 and 1.25 μgm^{-3} in the winter and summer seasons, respectively), are associated with emissions from agriculture–livestock, mainly due to differences in particulate nitrate (PNO_3) concentrations.

- Finally, modeling of gas-aerosol partitioning and chemical aging of organic aerosol using the 1.5-D VBS scheme and including the estimations of I/SVOCs emissions within the VBS experiment, compared to the use of the SOAP scheme, is mainly manifested by an increase in the average seasonal impacts on the concentration of $PM_{2.5}$ caused by emissions from other stationary combustion and road transport during the winter seasons (reaching up to 12 and 4 μgm^{-3}, respectively) and mainly by an increase in the average seasonal impact on the concentration of $PM_{2.5}$ produced by emissions from transport during the summer seasons (reaching up to 2.25 μgm^{-3}). Qualitatively, the same conclusions also apply to increases in the daily averages in the cities.

The results presented in this paper provide detailed and valuable information about the contributions of emissions from a broad spectrum of anthropogenic activities to the current composition of fine PM in Central Europe and its selected metropolises, as well as about the impacts of potential overall emission reductions within individual activity sectors on its composition. These can be used, at least as framework estimates, in designing appropriate strategies to reduce this kind of air pollution.

The above-discussed possible reasons leading to the shortcomings of the used model system in capturing the concentration of fine PM indicate our future activities (e.g., the inclusion of dust emissions within the scope of the domain and boundary conditions) to eliminate them potentially. In addition, an inherent aspect in the effort to improve the overall quality of model

https://doi.org/10.5194/egusphere-2023-1919
Preprint. Discussion started: 12 September 2023
© Author(s) 2023. CC BY 4.0 License.

experiments will be a significant increase in their resolution, at least as additional nested domains covering selected areas of interest (e.g., selected urban areas).

Appendix A: Definitions of average temporal impacts and contributions

Based on the principle of the zero-out method, we define the average temporal absolute impact of emissions from the sector of anthropogenic activity x on the concentration $c(i)$ of chemical species (or their aggregate) i as:

$$\overline{I_x^{\mathrm{abs}}(c(i))} = \frac{1}{N}\sum_{j=1}^{N}\left(c_j^{\mathrm{BASE}}(i) - c_j^{x}(i)\right), \tag{A1}$$

where $c_j^{\mathrm{BASE}}(i)$ and $c_j^{x}(i)$ are the average hourly concentrations of chemical species (or their aggregate) i in the base simulation and the perturbed simulation with zero emissions from sector x, respectively, falling within the appropriate time interval, and N is their total number. The average temporal relative impact of emissions from the sector of anthropogenic activity x on the concentration $c(i)$ of chemical species i (or their aggregate) is considered as:

$$\overline{I_x^{\mathrm{rel}}(c(i))} = 100\frac{\overline{I_x^{\mathrm{abs}}(c(i))}}{\frac{1}{N}\sum_{j=1}^{N} c_j^{\mathrm{BASE}}(\mathrm{PM}_{2.5})}, \tag{A2}$$

where $\overline{I_x^{\mathrm{abs}}(c(i))}$ is defined by Eq. (A1), $c_j^{\mathrm{BASE}}(\mathrm{PM}_{2.5})$ are the average hourly concentrations of $\mathrm{PM}_{2.5}$ in the base simulation falling within the appropriate time interval, and N is their total number. Thus, Eq. (A2) shows that $\overline{I_x^{\mathrm{rel}}(c(i))}$ defined by us represents the ratio between $\overline{I_x^{\mathrm{abs}}(c(i))}$ and the corresponding time-averaged concentration of $\mathrm{PM}_{2.5}$ in the base simulation, expressed as a percentage.

In connection with the source apportionment given by the PSAT tool, we define the average temporal absolute contribution of emissions from the given category x to the concentration $c(i)$ of chemical species (or their aggregate) i as:

$$\overline{C_x^{\mathrm{abs}}(c(i))} = \frac{1}{N}\sum_{j=1}^{N} c_j^{x}(i), \tag{A3}$$

where $c_j^{x}(i)$ are the average hourly concentrations of chemical species (or their aggregate) i allocated to the given category x by the PSAT tool that fall within the appropriate time interval, and N is their total number. It is worth mentioning here that the allocation in the PSAT experiment is realized into 15 categories (individual GNFR sectors A–L, biogenic emissions, initial condition, and boundary conditions). Finally, the average temporal relative contribution of emissions from the given category x to the concentration $c(i)$ of chemical species i (or their aggregate) is considered as:

$$\overline{C_x^{\mathrm{rel}}(c(i))} = 100\frac{\overline{C_x^{\mathrm{abs}}(c(i))}}{\overline{C_{\mathrm{tot}}^{\mathrm{abs}}(c(\mathrm{PM}_{2.5}))}}, \tag{A4}$$

where $\overline{C_x^{\mathrm{abs}}(c(i))}$ is defined by Eq. (A3), and $\overline{C_{\mathrm{tot}}^{\mathrm{abs}}(c(\mathrm{PM}_{2.5}))}$ represents the sum of $\overline{C_x^{\mathrm{abs}}(c(\mathrm{PM}_{2.5}))}$ over all 15 above mentioned categories. Thus, Eq. (A4) illustrates that $\overline{C_x^{\mathrm{rel}}(c(i))}$ defined by us represents the ratio between $\overline{C_x^{\mathrm{abs}}(c(i))}$ and the corresponding time-averaged concentration of $\mathrm{PM}_{2.5}$ in the PSAT experiment, expressed as a percentage.

https://doi.org/10.5194/egusphere-2023-1919
Preprint. Discussion started: 12 September 2023
© Author(s) 2023. CC BY 4.0 License.

Code and data availability. CAMx version 7.10 is available at http://camx-wp.azurewebsites.net/download/source (Ramboll, 2022). The WRF version 4.2 used in the study is available at https://github.com/wrf-model/WRF/releases (WRF, 2023)). The observational data from the AirBase database can be obtained from https://discomap.eea.europa.eu/map/fme/AirQualityExport.htm. (EEA, 2023). The CAMS emission data can be obtained from https://permalink.aeris-data.fr/CAMS-REG-ANT (Kuenen et al., 2021). The Czech REZZO and ATEM emission datas can be obtained upon request from their publishers, the Czech Hydrometeorological Institue (https://www.chmi.cz) and the Studio of Ecological Models (https://www.atem.cz). The complete model configuration and all the simulated data (3-dimensional hourly data) used for the analysis are stored at the Dept. of Atmospheric Physics of the Charles University data storage facilities (about 3TB) and are available upon request from the main author.

Author contributions. LB, KE, and JK performed the model simulations; LB and PH contributed to the data analysis and writing of the manuscript; OV conceptualized the study and planned the experiments.

Competing interests. No competing interests are present.

Acknowledgements. This work has been supported by the Czech Technological Agency (TACR) grant No.SS02030031 ARAMIS (Air Quality Research Assessment and Monitoring Integrated System) and Charles University SVV 260709 project.

https://doi.org/10.5194/egusphere-2023-1919
Preprint. Discussion started: 12 September 2023
© Author(s) 2023. CC BY 4.0 License.

References

Anderson, J. O., Thundiyil, J. G., and Stolbach, A.: Clearing the Air: A Review of the Effects of Particulate Matter Air Pollution on Human Health, Journal of Medical Toxicology, 8, 166–175, https://doi.org/10.1007/s13181-011-0203-1, 2012.

Apte, J. S., Marshall, J. D., Cohen, A. J., and Brauer, M.: Addressing Global Mortality from Ambient PM2.5, Environmental Science & Technology, 49, 8057–8066, https://doi.org/10.1021/acs.est.5b01236, 2015.

Arasa, R., Domingo-Dalmau, A., and Vargas, R.: Using a Coupled Air Quality Modeling System for the Development of an Air Quality Plan in Madrid (Spain): Source Apportionment and Analysis Evaluation of Mitigation Measures, Journal of Geoscience and Environment Protection, 4, 46–61, https://doi.org/10.4236/gep.2016.43005, 2016.

Benešová, N., Belda, M., Eben, K., Geletič, J., Huszár, P., Juruš, P., Krč, P., Resler, J., and Vlček, O.: New open source emission processor for air quality models, in: Proceedings of Abstracts 11th International Conference on Air Quality Science and Application, edited by Sokhi, R., Tiwari, P. R., Gállego, M. J., Craviotto Arnau, J. M., Castells Guiu, C., and Singh, V., p. 22, Published by University of Hertfordshire, https://doi.org/10.18745/PB.19829, paper presented at Air Quality 2018 conference, Barcelona, 12-16 March, 2018.

Bougeault, P. and Lacarrere, P.: Parameterization of orography-induced turbulence in a mesobeta-scale model, Monthly Weather Review, 117, 1872–1890, 1989.

Bove, M., Brotto, P., Cassola, F., Cuccia, E., Massabò, D., Mazzino, A., Piazzalunga, A., and Prati, P.: An integrated PM2.5 source apportionment study: Positive Matrix Factorisation vs. the chemical transport model CAMx, Atmospheric Environment, 94, 274–286, https://doi.org/10.1016/j.atmosenv.2014.05.039, 2014.

Bressi, M., Cavalli, F., Putaud, J., Fröhlich, R., Petit, J.-E., Aas, W., Äijälä, M., Alastuey, A., Allan, J., Aurela, M., Berico, M., Bougiatioti, A., Bukowiecki, N., Canonaco, F., Crenn, V., Dusanter, S., Ehn, M., Elsasser, M., Flentje, H., Graf, P., Green, D., Heikkinen, L., Hermann, H., Holzinger, R., Hueglin, C., Keernik, H., Kiendler-Scharr, A., Kubelová, L., Lunder, C., Maasikmets, M., Makeš, O., Malaguti, A., Mihalopoulos, N., Nicolas, J., O'Dowd, C., Ovadnevaite, J., Petralia, E., Poulain, L., Priestman, M., Riffault, V., Ripoll, A., Schlag, P., Schwarz, J., Sciare, J., Slowik, J., Sosedova, Y., Stavroulas, I., Teinemaa, E., Via, M., Vodička, P., Williams, P., Wiedensohler, A., Young, D., Zhang, S., Favez, O., Minguillón, M., and Prevot, A.: A European aerosol phenomenology - 7: High-time resolution chemical characteristics of submicron particulate matter across Europe, Atmospheric Environment: X, 10, 100 108, https://doi.org/10.1016/j.aeaoa.2021.100108, 2021.

Burr, M. J. and Zhang, Y.: Source apportionment of fine particulate matter over the Eastern U.S. Part II: source apportionment simulations using CAMx/PSAT and comparisons with CMAQ source sensitivity simulations, Atmospheric Pollution Research, 2, 318–336, https://doi.org/10.5094/APR.2011.037, 2011a.

Burr, M. J. and Zhang, Y.: Source apportionment of fine particulate matter over the Eastern U.S. Part I: source sensitivity simulations using CMAQ with the Brute Force method, Atmospheric Pollution Research, 2, 300–317, https://doi.org/10.5094/APR.2011.036, 2011b.

Byun, D. W. and Ching, J. K. S.: Science Algorithms of the EPA Model-3 Community Multiscale Air Quality (CMAQ) Modeling System, Office of Research and Development, U.S. EPA, North Carolina, 1999.

Chang, J. S., Brost, R. A., Isaksen, I. S. A., Madronich, S., Middleton, P., Stockwell, W. R., and Walcek, C. J.: A three-dimensional Eulerian acid deposition model: Physical concepts and formulation, Journal of Geophysical Research: Atmospheres, 92, 14 681–14 700, https://doi.org/10.1029/JD092iD12p14681, 1987.

© Author(s) 2023. CC BY 4.0 License.

Chen, F. and Dudhia, J.: Coupling an Advanced Land Surface–Hydrology Model with the Penn State–NCAR MM5 Modeling System. Part I: Model Implementation and Sensitivity, Monthly Weather Review, 129, 569–585, https://doi.org/10.1175/1520-0493(2001)129<0569:CAALSH>2.0.CO;2, 2001.

Chen, G., Canonaco, F., Tobler, A., Aas, W., Alastuey, A., Allan, J., Atabakhsh, S., Aurela, M., Baltensperger, U., Bougiatioti, A., De Brito, J. F., Ceburnis, D., Chazeau, B., Chebaicheb, H., Daellenbach, K. R., Ehn, M., El Haddad, I., Eleftheriadis, K., Favez, O., Flentje, H., Font, A., Fossum, K., Freney, E., Gini, M., Green, D. C., Heikkinen, L., Herrmann, H., Kalogridis, A.-C., Keernik, H., Lhotka, R., Lin, C., Lunder, C., Maasikmets, M., Manousakas, M. I., Marchand, N., Marin, C., Marmureanu, L., Mihalopoulos, N., Močnik, G., Nęcki, J., O'Dowd, C., Ovadnevaite, J., Peter, T., Petit, J.-E., Pikridas, M., Matthew Platt, S., Pokorná, P., Poulain, L., Priestman, M., Riffault, V., Rinaldi, M., Różański, K., Schwarz, J., Sciare, J., Simon, L., Skiba, A., Slowik, J. G., Sosedova, Y., Stavroulas, I., Styszko, K., Teinemaa, E., Timonen, H., Tremper, A., Vasilescu, J., Via, M., Vodička, P., Wiedensohler, A., Zografou, O., Cruz Minguillón, M., and Prévôt, A. S.: European aerosol phenomenology - 8: Harmonised source apportionment of organic aerosol using 22 Year-long ACSM/AMS datasets, Environment International, 166, 107 325, https://doi.org/10.1016/j.envint.2022.107325, 2022.

Ciarelli, G., Aksoyoglu, S., El Haddad, I., Bruns, E. A., Crippa, M., Poulain, L., Äijälä, M., Carbone, S., Freney, E., O'Dowd, C., Baltensperger, U., and Prévôt, A. S. H.: Modelling winter organic aerosol at the European scale with CAMx: evaluation and source apportionment with a VBS parameterization based on novel wood burning smog chamber experiments, Atmospheric Chemistry and Physics, 17, 7653–7669, https://doi.org/10.5194/acp-17-7653-2017, 2017.

Clappier, A., Belis, C. A., Pernigotti, D., and Thunis, P.: Source apportionment and sensitivity analysis: two methodologies with two different purposes, Geoscientific Model Development, 10, 4245–4256, https://doi.org/10.5194/gmd-10-4245-2017, 2017.

Coelho, S., Ferreira, J., Rodrigues, V., and Lopes, M.: Source apportionment of air pollution in European urban areas: Lessons from the ClairCity project, Journal of Environmental Management, 320, 115 899, https://doi.org/10.1016/j.jenvman.2022.115899, 2022.

Denier van der Gon, H., Hendriks, C., Kuenen, J., Segers, A., and Visschedijk, A.: Description of current temporal emission patterns and sensitivity of predicted AQ for temporal emission patterns, EU FP7 MACC deliverable report D_D-EMIS_1.3, https://atmosphere.copernicus.eu/sites/default/files/2019-07/MACC_TNO_del_1_3_v2.pdf, last access: 25 January 2023, 2011.

Denier van der Gon, H. A. C., Bergström, R., Fountoukis, C., Johansson, C., Pandis, S. N., Simpson, D., and Visschedijk, A. J. H.: Particulate emissions from residential wood combustion in Europe – revised estimates and an evaluation, Atmospheric Chemistry and Physics, 15, 6503–6519, https://doi.org/10.5194/acp-15-6503-2015, 2015.

Donahue, N. M., Robinson, A. L., Stanier, C. O., and Pandis, S. N.: Coupled Partitioning, Dilution, and Chemical Aging of Semivolatile Organics, Environmental Science & Technology, 40, 2635–2643, https://doi.org/10.1021/es052297c, 2006.

Donahue, N. M., Epstein, S. A., Pandis, S. N., and Robinson, A. L.: A two-dimensional volatility basis set: 1. organic-aerosol mixing thermodynamics, Atmospheric Chemistry and Physics, 11, 3303–3318, https://doi.org/10.5194/acp-11-3303-2011, 2011.

Donahue, N. M., Kroll, J. H., Pandis, S. N., and Robinson, A. L.: A two-dimensional volatility basis set – Part 2: Diagnostics of organic-aerosol evolution, Atmospheric Chemistry and Physics, 12, 615–634, https://doi.org/10.5194/acp-12-615-2012, 2012.

EEA: Air quality in Europe 2022, Report no. 05/2022, https://www.eea.europa.eu//publications/air-quality-in-europe-2022, last access: 25 January 2023, 2022.

EEA: Air Quality e-Reporting products on EEA data service: E1a and E2a data sets, European Environment Agency, Copenhagen, Denmark [data set], https://discomap.eea.europa.eu/map/fme/AirQualityExport.htm, last access: 25 January 2023, 2023.

EPA: CMAQ User's Guide, United States Environmental Protection Agency (U.S. EPA), available at: https://www.epa.gov/cmaq (last access: 25 January 2023), 2022.

https://doi.org/10.5194/egusphere-2023-1919
Preprint. Discussion started: 12 September 2023
© Author(s) 2023. CC BY 4.0 License.

Fountoukis, C., Racherla, P. N., Denier van der Gon, H. A. C., Polymeneas, P., Charalampidis, P. E., Pilinis, C., Wiedensohler, A., Dall'Osto, M., O'Dowd, C., and Pandis, S. N.: Evaluation of a three-dimensional chemical transport model (PMCAMx) in the European domain during the EUCAARI May 2008 campaign, Atmospheric Chemistry and Physics, 11, 10 331–10 347, https://doi.org/10.5194/acp-11-10331-2011, 2011.

Giani, P., Balzarini, A., Pirovano, G., Gilardoni, S., Paglione, M., Colombi, C., Gianelle, V. L., Belis, C. A., Poluzzi, V., and Lonati, G.: Influence of semi- and intermediate-volatile organic compounds (S/IVOC) parameterizations, volatility distributions and aging schemes on organic aerosol modelling in winter conditions, Atmospheric Environment, 213, 11–24, https://doi.org/10.1016/j.atmosenv.2019.05.061, 2019.

Guenther, A. B., Jiang, X., Heald, C. L., Sakulyanontvittaya, T., Duhl, T., Emmons, L. K., and Wang, X.: The Model of Emissions of Gases and Aerosols from Nature version 2.1 (MEGAN2.1): an extended and updated framework for modeling biogenic emissions, Geoscientific Model Development, 5, 1471–1492, https://doi.org/10.5194/gmd-5-1471-2012, 2012.

Hendriks, C., Kranenburg, R., Kuenen, J., van Gijlswijk, R., Wichink Kruit, R., Segers, A., Denier van der Gon, H., and Schaap, M.: The origin of ambient particulate matter concentrations in the Netherlands, Atmospheric Environment, 69, 289–303, https://doi.org/10.1016/j.atmosenv.2012.12.017, 2013.

Hertel, O., Berkowicz, R., Christensen, J., and Hov, Ø.: Test of two numerical schemes for use in atmospheric transport-chemistry models, Atmospheric Environment. Part A. General Topics, 27, 2591–2611, https://doi.org/10.1016/0960-1686(93)90032-T, 1993.

Huszar, P., Karlický, J., Ďoubalová, J., Nováková, T., Šindelářová, K., Švábik, F., Belda, M., Halenka, T., and Žák, M.: The impact of urban land-surface on extreme air pollution over central Europe, Atmospheric Chemistry and Physics, 20, 11 655–11 681, https://doi.org/10.5194/acp-20-11655-2020, 2020a.

Huszar, P., Karlický, J., Ďoubalová, J., Šindelářová, K., Nováková, T., Belda, M., Halenka, T., Žák, M., and Pišoft, P.: Urban canopy meteorological forcing and its impact on ozone and $PM_{2.5}$: role of vertical turbulent transport, Atmospheric Chemistry and Physics, 20, 1977–2016, https://doi.org/10.5194/acp-20-1977-2020, 2020b.

Huszar, P., Karlický, J., Marková, J., Nováková, T., Liaskoni, M., and Bartík, L.: The regional impact of urban emissions on air quality in Europe: the role of the urban canopy effects, Atmospheric Chemistry and Physics, 21, 14 309–14 332, https://doi.org/10.5194/acp-21-14309-2021, 2021.

Iacono, M. J., Delamere, J. S., Mlawer, E. J., Shephard, M. W., Clough, S. A., and Collins, W. D.: Radiative forcing by longlived greenhouse gases: Calculations with the AER radiative transfer models, J. Geophys. Res., 113, 2–9, https://doi.org/10.1029/2008JD009944, 2008.

Jiang, J., Aksoyoglu, S., Ciarelli, G., Oikonomakis, E., El-Haddad, I., Canonaco, F., O'Dowd, C., Ovadnevaite, J., Minguillón, M. C., Baltensperger, U., and Prévôt, A. S. H.: Effects of two different biogenic emission models on modelled ozone and aerosol concentrations in Europe, Atmospheric Chemistry and Physics, 19, 3747–3768, https://doi.org/10.5194/acp-19-3747-2019, 2019a.

Jiang, J., Aksoyoglu, S., El-Haddad, I., Ciarelli, G., Denier van der Gon, H. A. C., Canonaco, F., Gilardoni, S., Paglione, M., Minguillón, M. C., Favez, O., Zhang, Y., Marchand, N., Hao, L., Virtanen, A., Florou, K., O'Dowd, C., Ovadnevaite, J., Baltensperger, U., and Prévôt, A. S. H.: Sources of organic aerosols in Europe: a modeling study using CAMx with modified volatility basis set scheme, Atmospheric Chemistry and Physics, 19, 15 247–15 270, https://doi.org/10.5194/acp-19-15247-2019, 2019b.

Jiang, J., El Haddad, I., Aksoyoglu, S., Stefenelli, G., Bertrand, A., Marchand, N., Canonaco, F., Petit, J.-E., Favez, O., Gilardoni, S., Baltensperger, U., and Prévôt, A. S. H.: Influence of biomass burning vapor wall loss correction on modeling organic aerosols in Europe by CAMx v6.50, Geoscientific Model Development, 14, 1681–1697, https://doi.org/10.5194/gmd-14-1681-2021, 2021.

https://doi.org/10.5194/egusphere-2023-1919
Preprint. Discussion started: 12 September 2023
© Author(s) 2023. CC BY 4.0 License.

Jiménez-Guerrero, P.: What Are the Sectors Contributing to the Exceedance of European Air Quality Standards over the Iberian Peninsula? A Source Contribution Analysis, Sustainability, 14, https://doi.org/10.3390/su14052759, 2022.

Juda-Rezler, K., Reizer, M., Maciejewska, K., Błaszczak, B., and Klejnowski, K.: Characterization of atmospheric PM2.5 sources at a Central European urban background site, Science of The Total Environment, 713, 136 729, https://doi.org/10.1016/j.scitotenv.2020.136729, 2020.

Kain, J. S.: The Kain–Fritsch Convective Parameterization: An Update, Journal of Applied Meteorology, 43, 170–181, 2004.

Karamchandani, P., Long, Y., Pirovano, G., Balzarini, A., and Yarwood, G.: Source-sector contributions to European ozone and fine PM in 2010 using AQMEII modeling data, Atmospheric Chemistry and Physics, 17, 5643–5664, https://doi.org/10.5194/acp-17-5643-2017, 2017.

Koo, B., Wilson, G. M., Morris, R. E., Dunker, A. M., and Yarwood, G.: Comparison of Source Apportionment and Sensitivity Analysis in a Particulate Matter Air Quality Model, Environmental Science & Technology, 43, 6669–6675, https://doi.org/10.1021/es9008129, 2009.

Koo, B., Knipping, E., and Yarwood, G.: 1.5-Dimensional volatility basis set approach for modeling organic aerosol in CAMx and CMAQ, Atmospheric Environment, 95, 158–164, https://doi.org/10.1016/j.atmosenv.2014.06.031, 2014.

Kranenburg, R., Segers, A. J., Hendriks, C., and Schaap, M.: Source apportionment using LOTOS-EUROS: module description and evaluation, Geoscientific Model Development, 6, 721–733, https://doi.org/10.5194/gmd-6-721-2013, 2013.

Kuenen, J., Dellaert, S., Visschedijk, A., Jalkanen, J.-P., Super, I., and Denier van der Gon, H.: Copernicus Atmosphere Monitoring Service regional emissions version 4.2 (CAMS-REG-v4.2), Copernicus Atmosphere Monitoring Service, ECCAD, https://doi.org/10.24380/0vzb-a387, 2021.

Kuenen, J. J. P., Visschedijk, A. J. H., Jozwicka, M., and Denier van der Gon, H. A. C.: TNO-MACC_II emission inventory; a multi-year (2003–2009) consistent high-resolution European emission inventory for air quality modelling, Atmospheric Chemistry and Physics, 14, 10 963–10 976, https://doi.org/10.5194/acp-14-10963-2014, 2014.

Lanz, V. A., Prévôt, A. S. H., Alfarra, M. R., Weimer, S., Mohr, C., DeCarlo, P. F., Gianini, M. F. D., Hueglin, C., Schneider, J., Favez, O., D'Anna, B., George, C., and Baltensperger, U.: Characterization of aerosol chemical composition with aerosol mass spectrometry in Central Europe: an overview, Atmospheric Chemistry and Physics, 10, 10 453–10 471, https://doi.org/10.5194/acp-10-10453-2010, 2010.

Liaskoni, M., Huszar, P., Bartík, L., Prieto Perez, A. P., Karlický, J., and Vlček, O.: Modelling the European wind-blown dust emissions and their impact on particulate matter (PM) concentrations, Atmospheric Chemistry and Physics, 23, 3629–3654, https://doi.org/10.5194/acp-23-3629-2023, 2023.

LMD: Chimere: Chemistry-transport model v2020r1 (Documentation), LMD/INERIS/LISA, available at: https://www.lmd.polytechnique.fr/chimere/ (last access: 25 January 2023), 2022.

Nenes, A., Pandis, S. N., and Pilinis, C.: ISORROPIA: A New Thermodynamic Equilibrium Model for Multiphase Multicomponent Inorganic Aerosols, Aquatic Geochemistry, 4, 123–152, https://doi.org/10.1023/A:1009604003981, 1998.

Nenes, A., Pandis, S. N., and Pilinis, C.: Continued development and testing of a new thermodynamic aerosol module for urban and regional air quality models, Atmospheric Environment, 33, 1553–1560, https://doi.org/10.1016/S1352-2310(98)00352-5, 1999.

Odum, J. R., Hoffmann, T., Bowman, F., Collins, D., Flagan, R. C., and Seinfeld, J. H.: Gas/particle partitioning and secondary organic aerosol yields, Environmental Science and Technology, 30, 2580–2585, https://doi.org/10.1021/es950943+, 1996.

Passant, N.: Speciation of UK Emissions of Non-methane Volatile Organic Compounds, DEFRA, Oxon, UK, https://uk-air.defra.gov.uk/assets/documents/reports/empire/AEAT_ENV_0545_final_v2.pdf, last access: 25 January 2023, 2002.

https://doi.org/10.5194/egusphere-2023-1919
Preprint. Discussion started: 12 September 2023
© Author(s) 2023. CC BY 4.0 License.

Pepe, N., Pirovano, G., Balzarini, A., Toppetti, A., Riva, G. M., Amato, F., and Lonati, G.: Enhanced CAMx source apportionment analysis at an urban receptor in Milan based on source categories and emission regions, Atmospheric Environment: X, 2, 100 020, https://doi.org/10.1016/j.aeaoa.2019.100020, 2019.

Putaud, J.-P., Van Dingenen, R., Alastuey, A., Bauer, H., Birmili, W., Cyrys, J., Flentje, H., Fuzzi, S., Gehrig, R., Hansson, H. C., Harrison, R. M., Herrmann, H., Hitzenberger, R., Hüglin, C., Jones, A. M., Kasper-Giebl, A., Kiss, G., Kousa, A., Kuhlbusch, T. A. J., Löschau, G., Maenhaut, W., Molnar, A., Moreno, T., Pekkanen, J., Perrino, C., Pitz, M., Puxbaum, H., Querol, X., Rodriguez, S., Salma, I., Schwarz, J., Smolik, J., Schneider, J., Spindler, G., ten Brink, H., Tursic, J., Viana, M., Wiedensohler, A., and Raes, F.: A European aerosol phenomenology – 3: Physical and chemical characteristics of particulate matter from 60 rural, urban, and kerbside sites across Europe, Atmospheric Environment, 44, 1308–1320, https://doi.org/10.1016/j.atmosenv.2009.12.011, 2010.

Pültz, J., Banzhaf, S., Thürkow, M., Kranenburg, R., and Schaap, M.: Source attribution of particulate matter in Berlin, Atmospheric Environment, 292, 119 416, https://doi.org/10.1016/j.atmosenv.2022.119416, 2023.

Ramboll: CAMx User's Guide, Comprehensive Air Quality model with Extentions, version 7.20, Novato, California, available at: http://www.camx.com (last access: 25 January 2023), 2022.

Robinson, A. L., Donahue, N. M., Shrivastava, M. K., Weitkamp, E. A., Sage, A. M., Grieshop, A. P., Lane, T. E., Pierce, J. R., and Pandis, S. N.: Rethinking Organic Aerosols: Semivolatile Emissions and Photochemical Aging, Science, 315, 1259–1262, https://doi.org/10.1126/science.1133061, 2007.

Schaap, M., Timmermans, R. M., Roemer, M., Boersen, G., Builtjes, P., Sauter, F., Velders, G., and Beck, J.: The LOTOS-EUROS model: description, validation and latest developments, International Journal of Environment and Pollution, 32, 270–290, https://doi.org/10.1504/IJEP.2008.017106, 2008.

Schneider, C., Pelzer, M., Toenges-Schuller, N., Nacken, M., and Niederau, A.: ArcGIS basierte Lösung zur detaillierten, deutschlandweiten Verteilung (Gridding) nationaler Emissionsjahreswerte auf Basis des Inventars zur Emissionsberichterstattung, Dessau. Roßlau Retrieved, 27, 2019, 2016.

Schwarz, J., Cusack, M., Karban, J., Chalupníčková, E., Havránek, V., Smolík, J., and Ždímal, V.: PM2.5 chemical composition at a rural background site in Central Europe, including correlation and air mass back trajectory analysis, Atmospheric Research, 176-177, 108–120, https://doi.org/10.1016/j.atmosres.2016.02.017, 2016.

Seinfeld, J. H. and Pandis, S. N.: Atmospheric Chemistry and Physics: From Air Pollution to Climate Change, Wiley, New York, 1998.

Simmons, A. J., Willett, K. M., Jones, P. D., Thorne, P. W., and Dee, D. P.: Low-frequency variations in surface atmospheric humidity, temperature, and precipitation: Inferences from reanalyses and monthly gridded observational data sets, Journal of Geophysical Research: Atmospheres, 115, D01 110, https://doi.org/10.1029/2009JD012442, 2010.

Sindelarova, K., Granier, C., Bouarar, I., Guenther, A., Tilmes, S., Stavrakou, T., Müller, J.-F., Kuhn, U., Stefani, P., and Knorr, W.: Global data set of biogenic VOC emissions calculated by the MEGAN model over the last 30 years, Atmospheric Chemistry and Physics, 14, 9317–9341, https://doi.org/10.5194/acp-14-9317-2014, 2014.

Skamarock, W. C., Klemp, J. B., Dudhia, J., Gill, D. O., Liu, Z., Berner, J., Wang, W., Powers, J. G., Duda, M. G., Barker, D., and Huang, X.: A Description of the Advanced Research WRF Version 4, NCAR Tech. Note NCAR/TN-556+STR, http://dx.doi.org/10.5065/1dfh-6p97, last access: 25 January 2023, 2019.

Skyllakou, K., Murphy, B. N., Megaritis, A. G., Fountoukis, C., and Pandis, S. N.: Contributions of local and regional sources to fine PM in the megacity of Paris, Atmospheric Chemistry and Physics, 14, 2343–2352, https://doi.org/10.5194/acp-14-2343-2014, 2014.

https://doi.org/10.5194/egusphere-2023-1919
Preprint. Discussion started: 12 September 2023
© Author(s) 2023. CC BY 4.0 License.

Skyllakou, K., Fountoukis, C., Charalampidis, P., and Pandis, S. N.: Volatility-resolved source apportionment of primary and secondary organic aerosol over Europe, Atmospheric Environment, 167, 1–10, https://doi.org/10.1016/j.atmosenv.2017.08.005, 2017.

Strader, R., Lurmann, F. W., and Pandis, S. N.: Evaluation of secondary organic aerosol formation in winter, Atmospheric Environment, 33, 4849–4863, 1999.

Szigeti, T., Óvári, M., C., D., Kelly, F. J., Lucarelli, F., and Záray, G.: Changes in chemical composition and oxidative potential of urban PM2.5 between 2010 and 2013 in Hungary, Science of The Total Environment, 518-519, 534–544, https://doi.org/10.1016/j.scitotenv.2015.03.025, 2015.

Tagaris, E., Sotiropoulou, R. E. P., Gounaris, N., Andronopoulos, S., and Vlachogiannis, D.: Effect of the Standard Nomenclature for Air Pollution (SNAP) Categories on Air Quality over Europe, Atmosphere, 6, 1119–1128, https://doi.org/10.3390/atmos6081119, 2015.

Thompson, G., Field, P. R., Rasmussen, R. M., and Hall, W. D.: Explicit Forecasts of Winter Precipitation Using an Improved Bulk Microphysics Scheme. Part II: Implementation of a New Snow Parameterization, Monthly Weather Review, 136, 5095–5115, https://doi.org/10.1175/2008MWR2387.1, 2008.

Turner, M. C., Andersen, Z. J., Baccarelli, A., Diver, W. R., Gapstur, S. M., Pope III, C. A., Prada, D., Samet, J., Thurston, G., and Cohen, A.: Outdoor air pollution and cancer: An overview of the current evidence and public health recommendations, CA: A Cancer Journal for Clinicians, 70, 460–479, https://doi.org/10.3322/caac.21632, 2020.

Wagstrom, K. M., Pandis, S. N., Yarwood, G., Wilson, G. M., and Morris, R. E.: Development and application of a computationally efficient particulate matter apportionment algorithm in a three-dimensional chemical transport model, Atmospheric Environment, 42, 5650–5659, https://doi.org/10.1016/j.atmosenv.2008.03.012, 2008.

Wang, Z. S., Chien, C.-J., and Tonnesen, G. S.: Development of a tagged species source apportionment algorithm to characterize three-dimensional transport and transformation of precursors and secondary pollutants, Journal of Geophysical Research: Atmospheres, 114, https://doi.org/10.1029/2008JD010846, 2009.

WRF: Weather Research and Forecast model code, version 4.0 source code, WRF [code], https://github.com/wrf-model/WRF/releases, last access: 25 January 2023, 2023.

Yarwood, G., Morris, R. E., and Wilson, G. M.: Particulate matter source apportionment technology (PSAT) in the CAMx photochemical grid model, Air Pollution Modeling and Its Application XVII, p. 478–492, https://www.scopus.com/inward/record.uri?eid=2s2.0-79957754586&partnerID=40&md5=bc9ad0a93221cfe81ccd37b9188d517d, 2007.

Yarwood, G., Jung, J., Whitten, G. Z., Heo, G., Mellberg, J., and Estes, E.: Updates to the Carbon Bond Mechanism for Version 6 (CB6), Presented at the 9th Annual CMAS Conference, Chapel Hill, https://www.cmascenter.org/conference/2010/abstracts/emery_updates_carbon_2010.pdf, last access: 25 January 2023, 2010.

Zhang, L., Gong, S., Padro, J., and Barrie, L.: A size-segregated particle dry deposition scheme for an atmospheric aerosol module, Atmospheric Environment, 35, 549–560, https://doi.org/10.1016/S1352-2310(00)00326-5, 2001.

Zhang, L., Brook, J. R., and Vet, R.: A revised parameterization for gaseous dry deposition in air-quality models, Atmospheric Chemistry and Physics, 3, 2067–2082, https://doi.org/10.5194/acp-3-2067-2003, 2003.

Zhao, Y., Nguyen, N. T., Presto, A. A., Hennigan, C. J., May, A. A., and Robinson, A. L.: Intermediate Volatility Organic Compound Emissions from On-Road Diesel Vehicles: Chemical Composition, Emission Factors, and Estimated Secondary Organic Aerosol Production, Environmental Science & Technology, 49, 11 516–11 526, https://doi.org/10.1021/acs.est.5b02841, 2015.

https://doi.org/10.5194/egusphere-2023-1919
Preprint. Discussion started: 12 September 2023
© Author(s) 2023. CC BY 4.0 License.

Zhao, Y., Nguyen, N. T., Presto, A. A., Hennigan, C. J., May, A. A., and Robinson, A. L.: Intermediate Volatility Organic Compound
1105 Emissions from On-Road Gasoline Vehicles and Small Off-Road Gasoline Engines, Environmental Science & Technology, 50, 4554–4563, https://doi.org/10.1021/acs.est.5b06247, 2016.

https://doi.org/10.5194/egusphere-2023-1919
Preprint. Discussion started: 12 September 2023
© Author(s) 2023. CC BY 4.0 License.

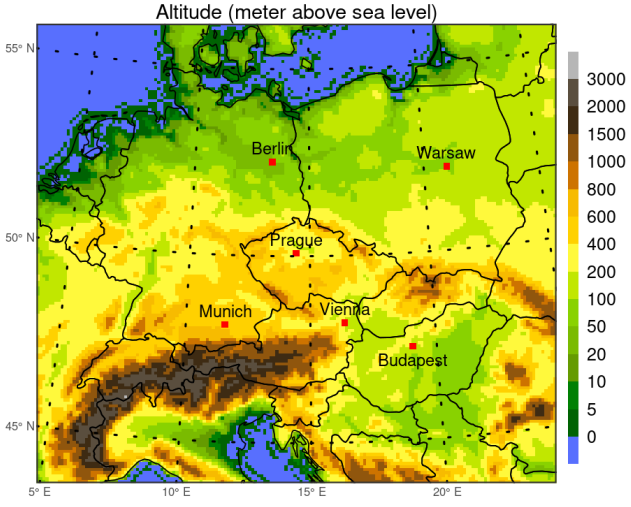

Figure 1. The resolved model terrain altitude (in meters above sea level) and the locations of the cities analyzed in the study (Prague, Berlin, Munich, Vienna, Budapest, Warsaw).

https://doi.org/10.5194/egusphere-2023-1919
Preprint. Discussion started: 12 September 2023
© Author(s) 2023. CC BY 4.0 License.

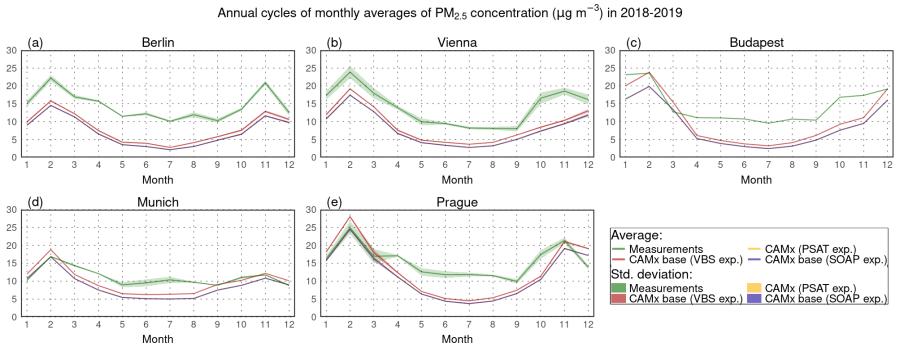

Figure 2. Comparison of modeled (the base simulation of the SOAP/VBS experiment – blue/red lines, the simulation of the PSAT experiment – orange lines) and measured (AirBase data – green lines) annual cycles of average monthly concentrations of $PM_{2.5}$ (in $\mu g m^{-3}$) in 2018–2019 at suburban and urban stations in Berlin **(a)**, Vienna **(b)**, Budapest **(c)**, Munich **(d)**, and Prague **(e)**. The colored areas indicate the standard deviations of the averages, calculated using Eq. (S4) provided in the Supplement. Their color scale corresponds to the scale used for the averages.

https://doi.org/10.5194/egusphere-2023-1919
Preprint. Discussion started: 12 September 2023
© Author(s) 2023. CC BY 4.0 License.

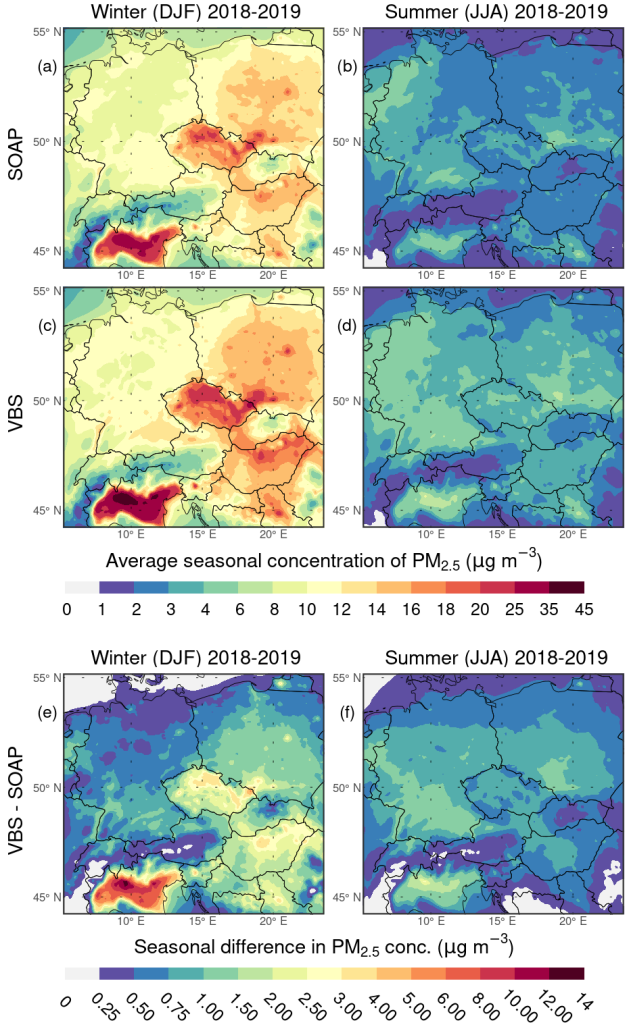

Figure 3. Comparison of average seasonal concentrations of $PM_{2.5}$ (in $\mu g m^{-3}$) in the base simulations of the SOAP **(a, b)** and VBS **(c, d)** experiments during the winter (DJF, **(a, c)**) and summer (JJA, **(b, d)**) seasons of 2018–2019. Panels **(e)** and **(f)** show the differences between seasonal $PM_{2.5}$ concentrations in the base simulation of the VBS and SOAP experiments during the winter and summer seasons, respectively.

https://doi.org/10.5194/egusphere-2023-1919
Preprint. Discussion started: 12 September 2023
© Author(s) 2023. CC BY 4.0 License.

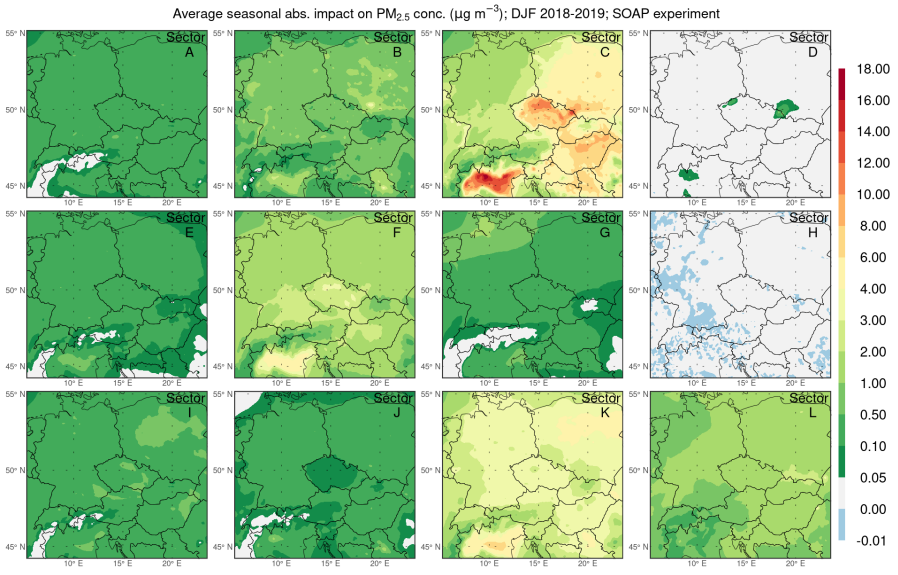

Figure 4. Spatial distributions of the average seasonal absolute impact of emissions from individual GNFR sectors A–L (indicated in the upper right corner of the panels) on the concentration of $PM_{2.5}$ (in $\mu g m^{-3}$) during the winter (DJF) seasons of 2018–2019 in the SOAP experiment.

https://doi.org/10.5194/egusphere-2023-1919
Preprint. Discussion started: 12 September 2023
© Author(s) 2023. CC BY 4.0 License.

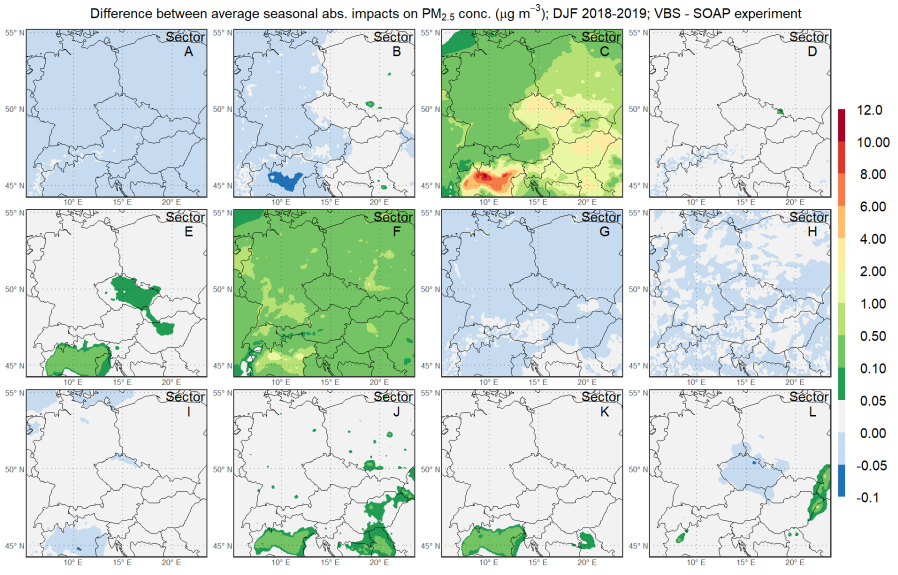

Figure 5. Spatial distributions of the differences between the average seasonal absolute impacts of emissions from individual GNFR sectors A–L (indicated in the upper right corner of the panels) on the concentration of $PM_{2.5}$ (in $\mu g m^{-3}$) in the VBS and SOAP experiments during the winter (DJF) seasons of 2018–2019.

https://doi.org/10.5194/egusphere-2023-1919
Preprint. Discussion started: 12 September 2023
© Author(s) 2023. CC BY 4.0 License.

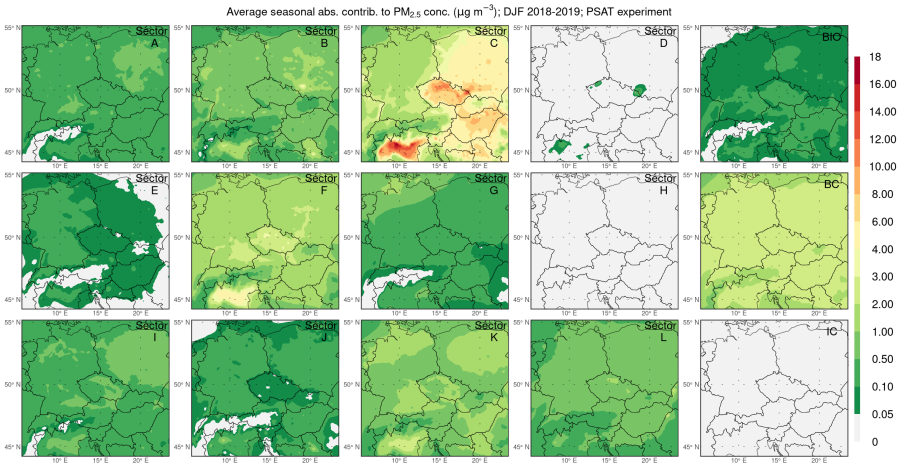

Figure 6. Spatial distributions of the average seasonal absolute contribution of emissions from individual categories (indicated in the upper right corner of the panels) to the concentration of $PM_{2.5}$ (in $\mu g m^{-3}$) during the winter (DJF) seasons of 2018–2019 in the PSAT experiment. Categories used: GNFR sectors A–L, BIO – biogenic emissions, BC – boundary conditions, IC – initial condition.

https://doi.org/10.5194/egusphere-2023-1919
Preprint. Discussion started: 12 September 2023
© Author(s) 2023. CC BY 4.0 License.

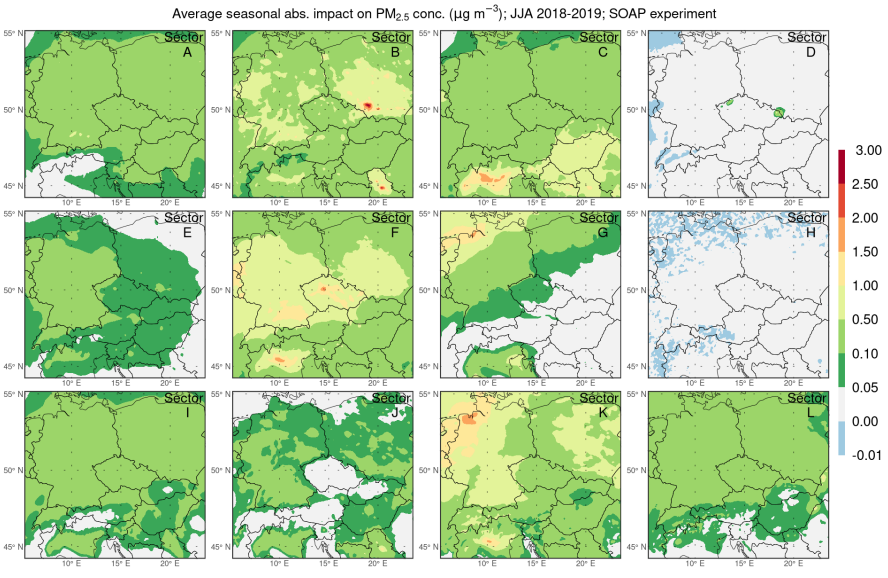

Figure 7. Same as Fig. 4 but for the summer (JJA) seasons of 2018–2019.

https://doi.org/10.5194/egusphere-2023-1919
Preprint. Discussion started: 12 September 2023
© Author(s) 2023. CC BY 4.0 License.

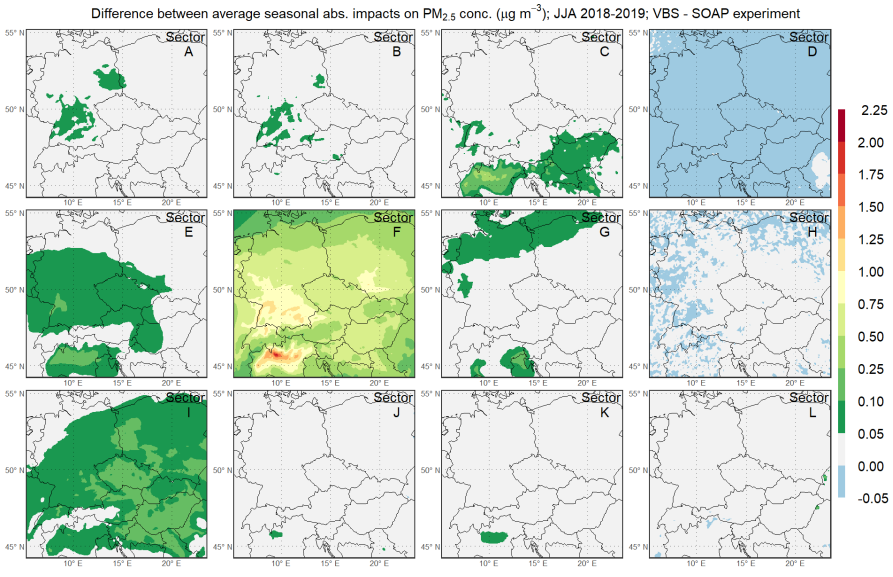

Figure 8. Same as Fig. 5 but for the summer (JJA) seasons of 2018–2019.

https://doi.org/10.5194/egusphere-2023-1919
Preprint. Discussion started: 12 September 2023
© Author(s) 2023. CC BY 4.0 License.

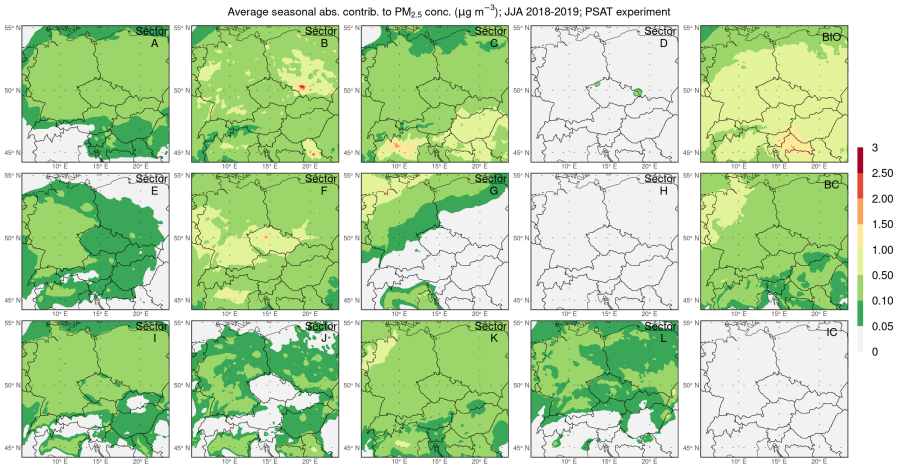

Figure 9. Same as Fig. 6 but for the summer (JJA) seasons of 2018–2019.

https://doi.org/10.5194/egusphere-2023-1919
Preprint. Discussion started: 12 September 2023
© Author(s) 2023. CC BY 4.0 License.

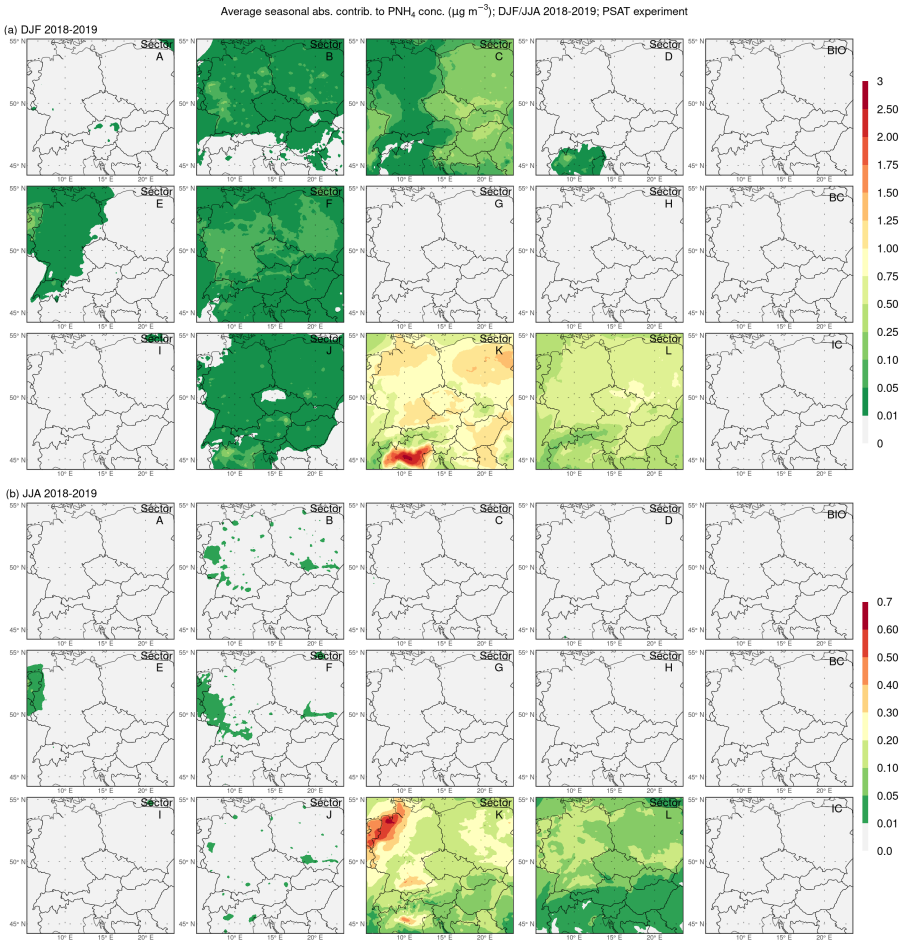

Figure 10. Spatial distributions of the average seasonal absolute contribution of emissions from individual categories (indicated in the upper right corner of the subpanels) to the concentration of PNH_4 (in $\mu g m^{-3}$) during the winter (DJF, **(a)**) and summer (JJA, **(b)**) seasons of 2018–2019 in the PSAT experiment. Categories used: GNFR sectors A–L, BIO – biogenic emissions, BC – boundary conditions, IC – initial condition.

https://doi.org/10.5194/egusphere-2023-1919
Preprint. Discussion started: 12 September 2023
© Author(s) 2023. CC BY 4.0 License.

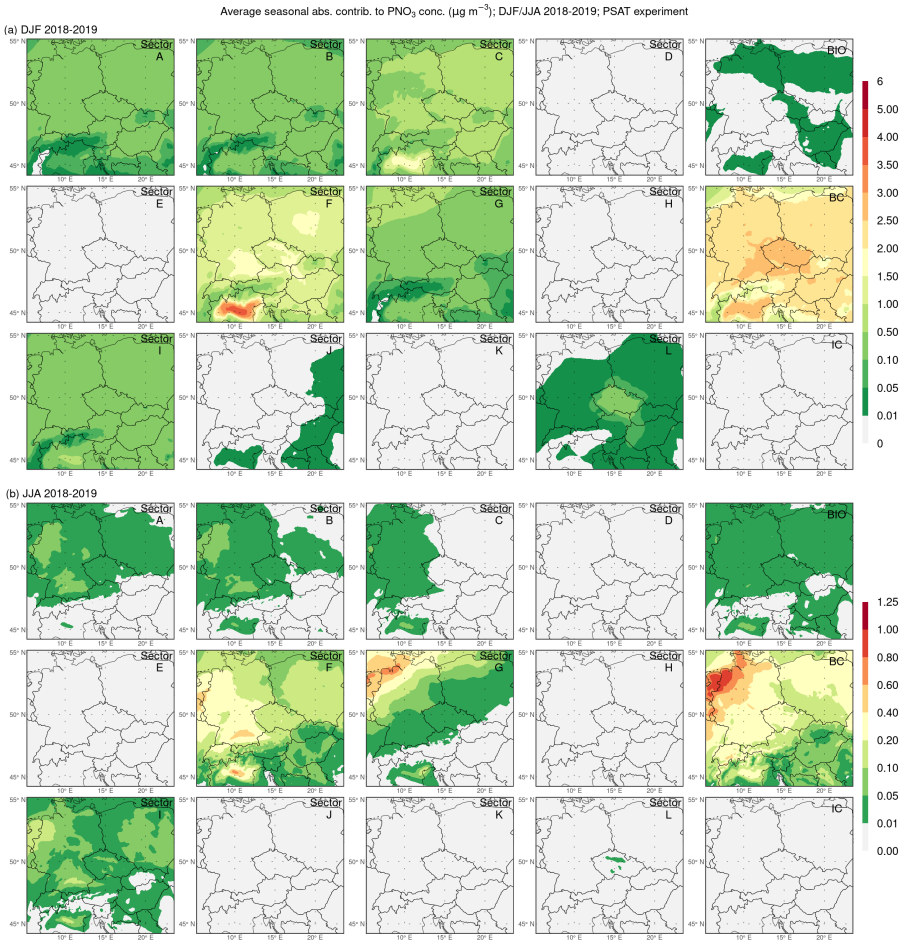

Figure 11. Same as Fig. 10 but for PNO_3.

https://doi.org/10.5194/egusphere-2023-1919
Preprint. Discussion started: 12 September 2023
© Author(s) 2023. CC BY 4.0 License.

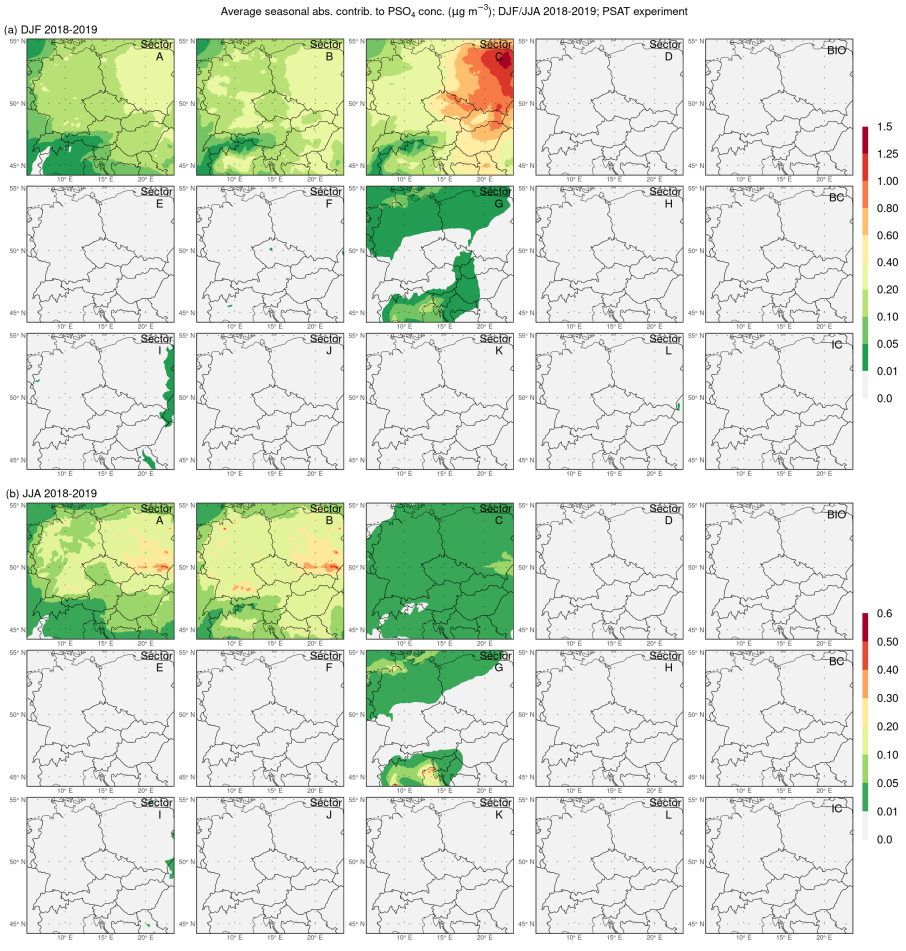

Figure 12. Same as Fig. 10 but for PSO_4.

https://doi.org/10.5194/egusphere-2023-1919
Preprint. Discussion started: 12 September 2023
© Author(s) 2023. CC BY 4.0 License.

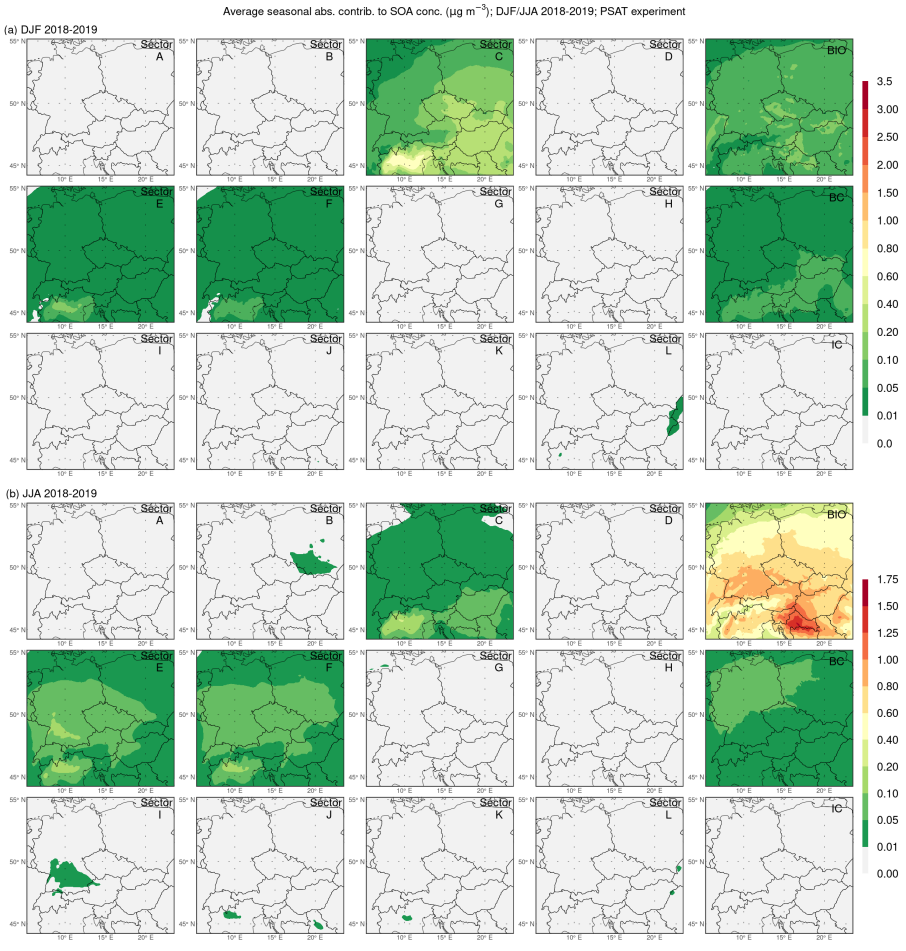

Figure 13. Same as Fig. 10 but for SOA.

https://doi.org/10.5194/egusphere-2023-1919
Preprint. Discussion started: 12 September 2023
© Author(s) 2023. CC BY 4.0 License.

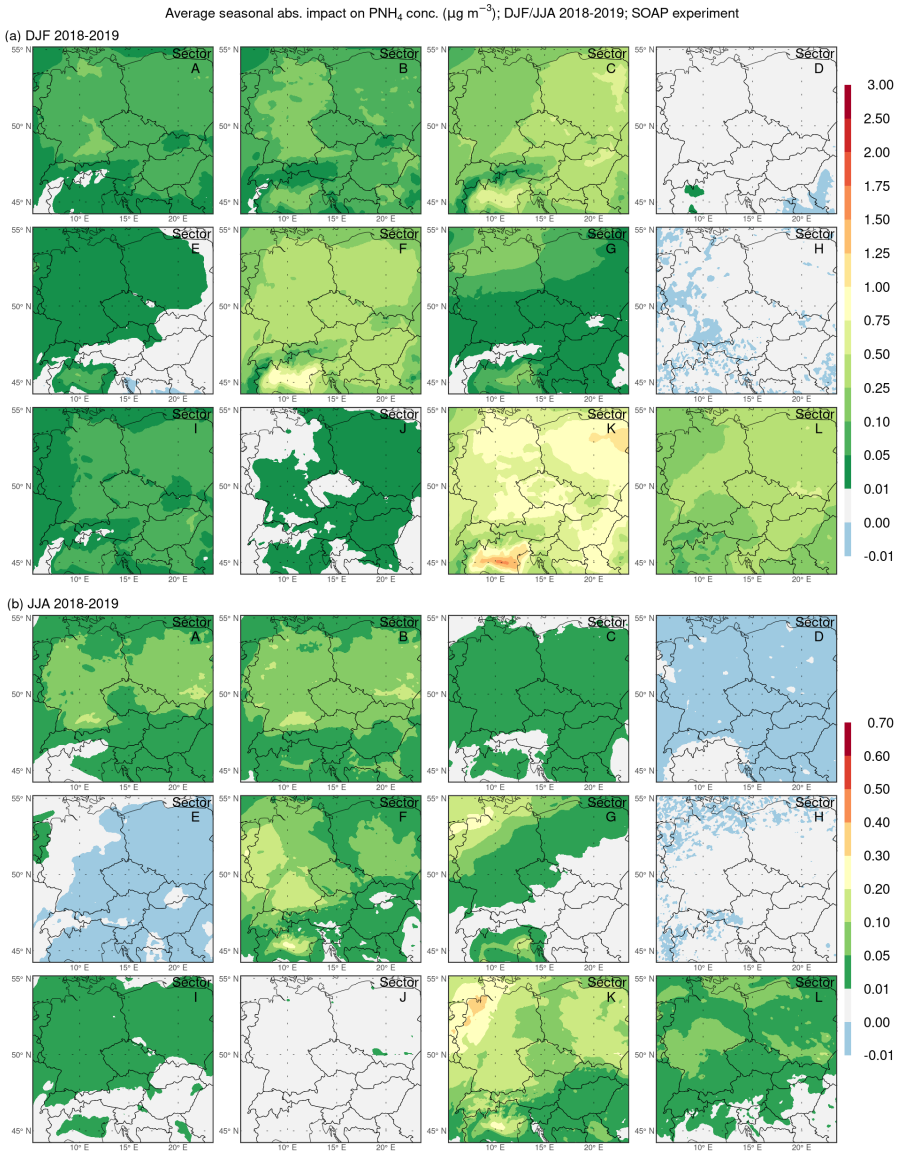

Figure 14. Spatial distributions of the average seasonal absolute impact of emissions from individual GNFR sectors A–L (indicated in the upper right corner of the subpanels) on the concentration of PNH_4 (in $\mu g m^{-3}$) during the winter (DJF, **(a)**) and summer (JJA, **(b)**) seasons of 2018–2019 in the SOAP experiment.

https://doi.org/10.5194/egusphere-2023-1919
Preprint. Discussion started: 12 September 2023
© Author(s) 2023. CC BY 4.0 License.

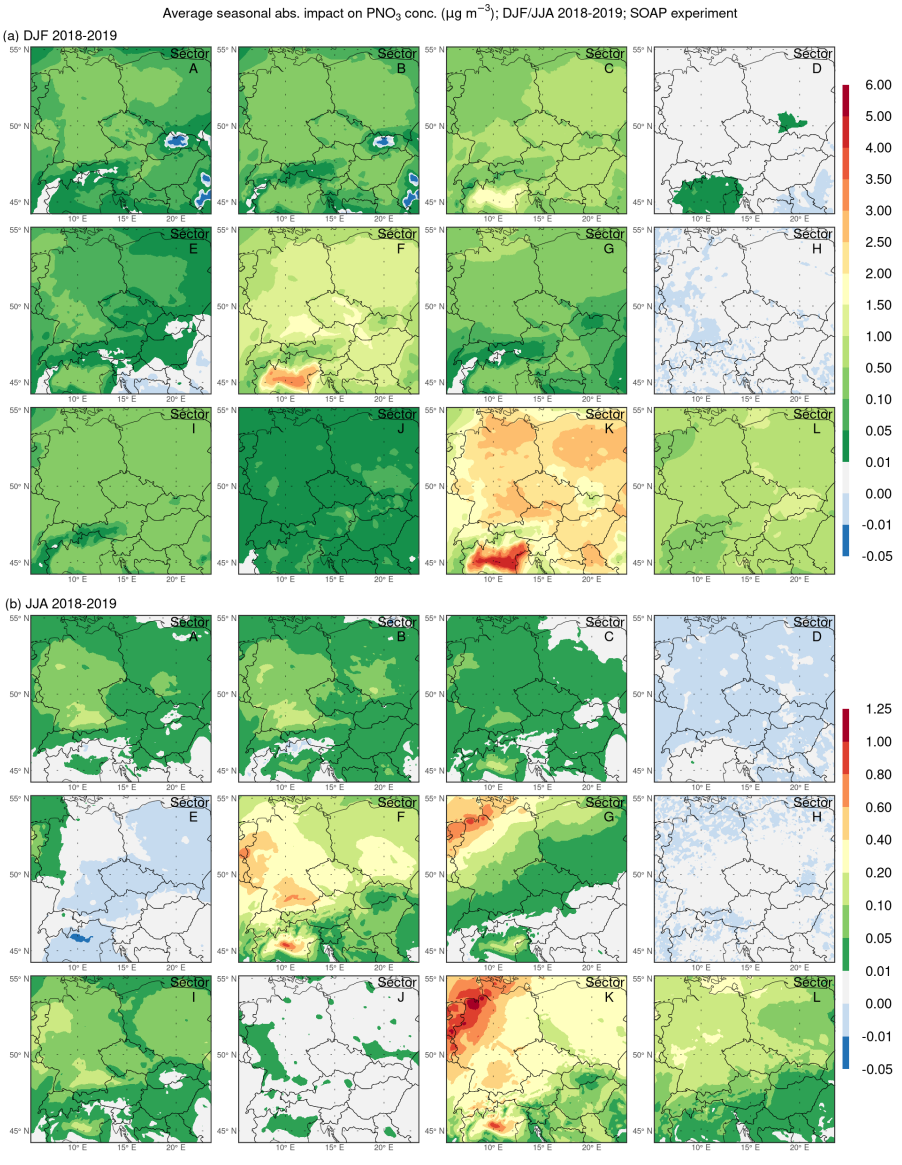

Figure 15. Same as Fig. 14 but for PNO_3.

https://doi.org/10.5194/egusphere-2023-1919
Preprint. Discussion started: 12 September 2023
© Author(s) 2023. CC BY 4.0 License.

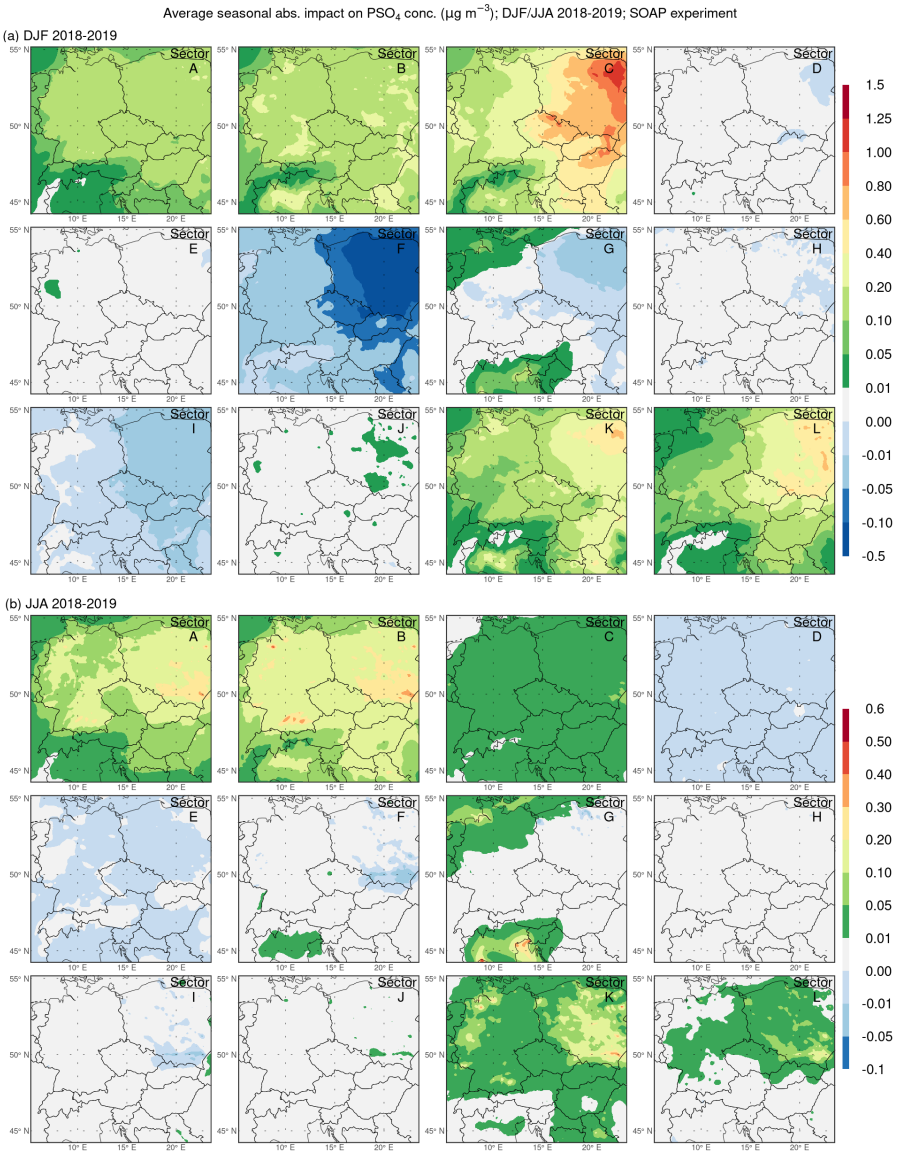

Figure 16. Same as Fig. 14 but for PSO_4.

https://doi.org/10.5194/egusphere-2023-1919
Preprint. Discussion started: 12 September 2023
© Author(s) 2023. CC BY 4.0 License.

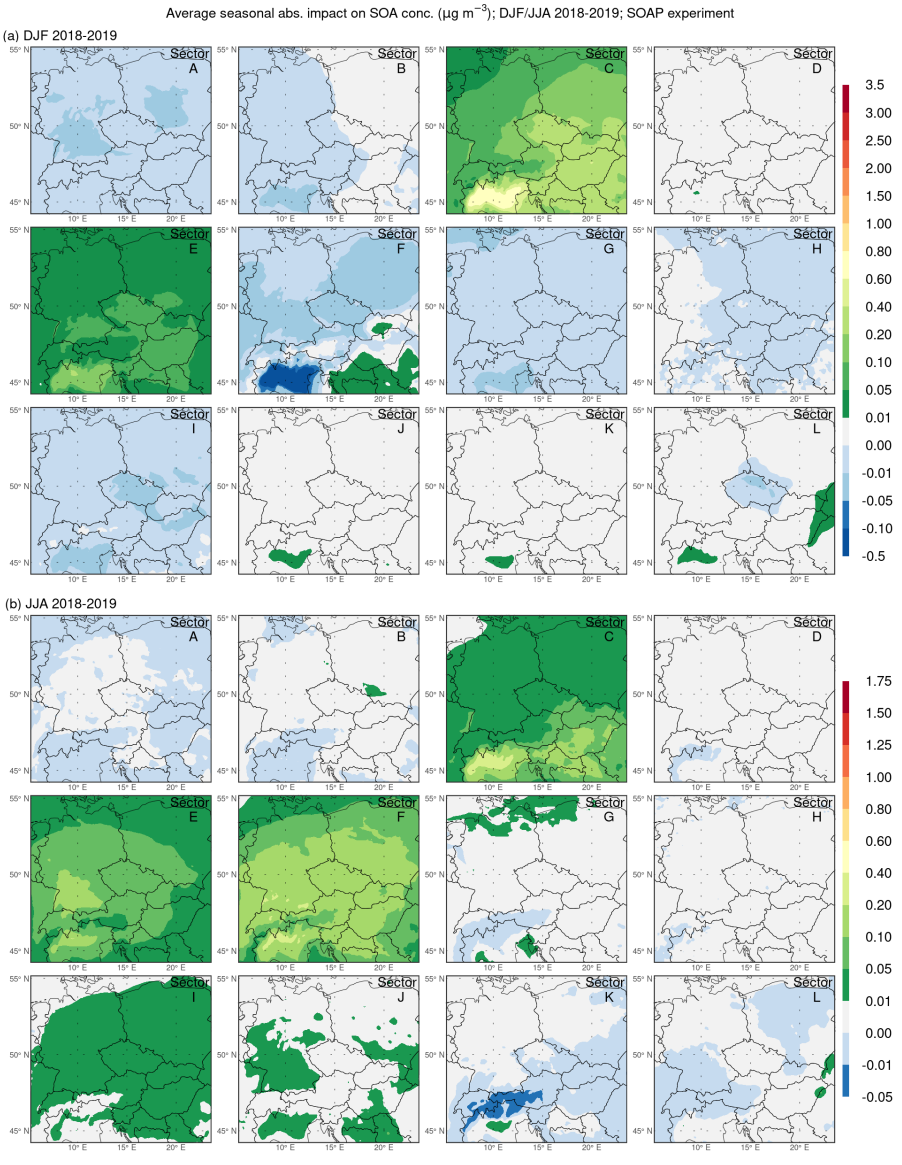

Figure 17. Same as Fig. 14 but for SOA.

https://doi.org/10.5194/egusphere-2023-1919
Preprint. Discussion started: 12 September 2023
© Author(s) 2023. CC BY 4.0 License.

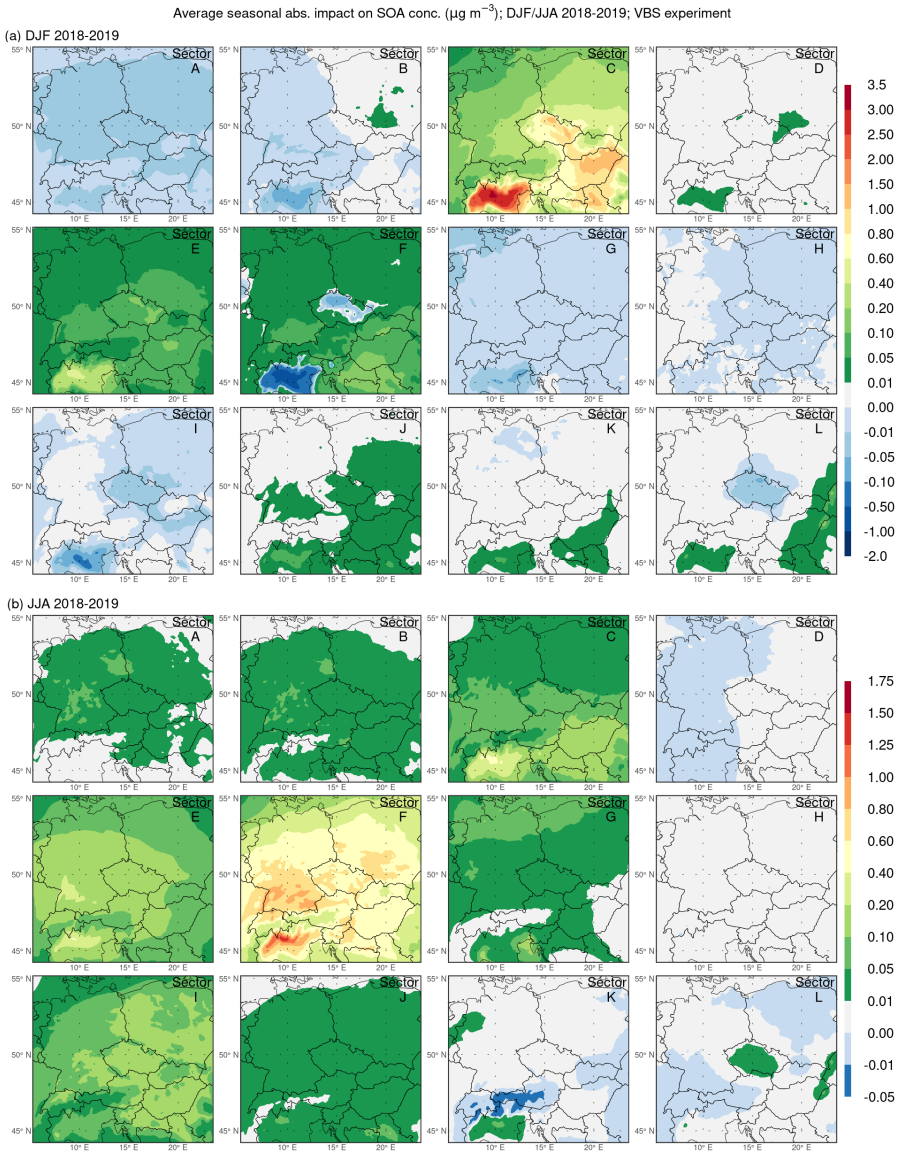

Figure 18. Same as Fig. 17 but for the VBS experiment.

https://doi.org/10.5194/egusphere-2023-1919
Preprint. Discussion started: 12 September 2023
© Author(s) 2023. CC BY 4.0 License.

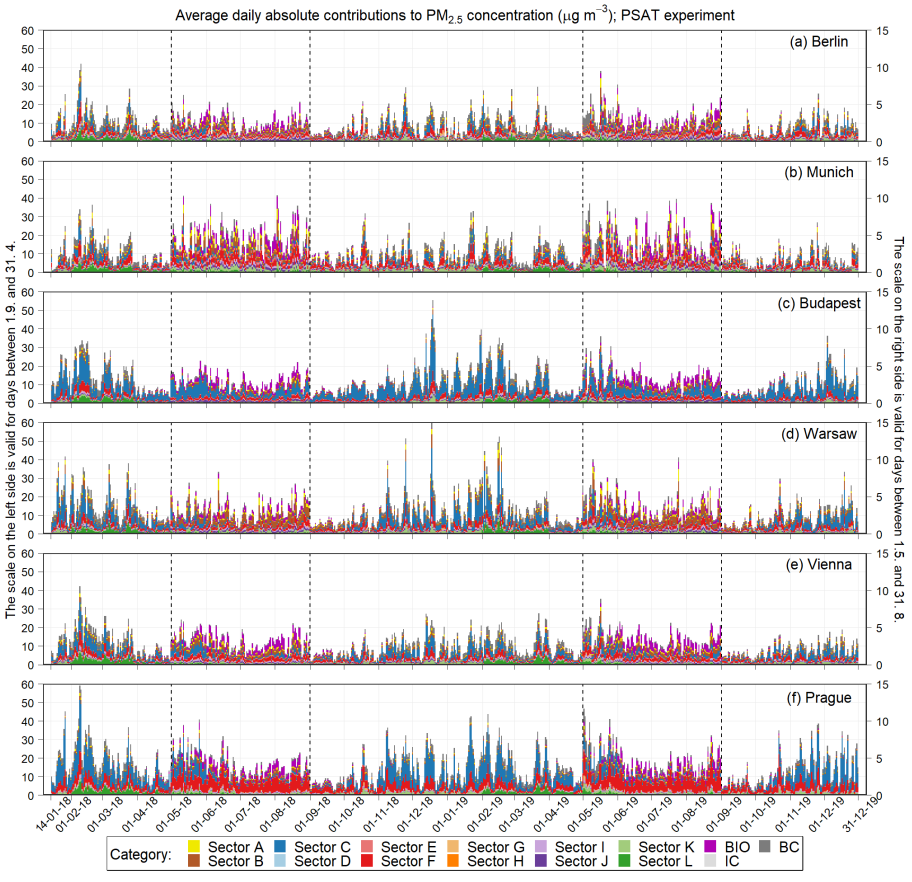

Figure 19. Temporal evolution of the average daily absolute contributions of emissions from individual categories to the concentration of $PM_{2.5}$ (in $\mu g m^{-3}$) above Berlin **(a)**, Munich **(b)**, Budapest **(c)**, Warsaw **(d)**, Vienna **(e)**, and Prague **(f)** in the PSAT experiment. Categories used: GNFR sectors A–L, BIO – biogenic emissions, BC – boundary conditions, IC – initial condition. The scale on the left (right) side is valid for the days between 1.9. and 31.4. (1.5. and 31.8.).

https://doi.org/10.5194/egusphere-2023-1919
Preprint. Discussion started: 12 September 2023
© Author(s) 2023. CC BY 4.0 License.

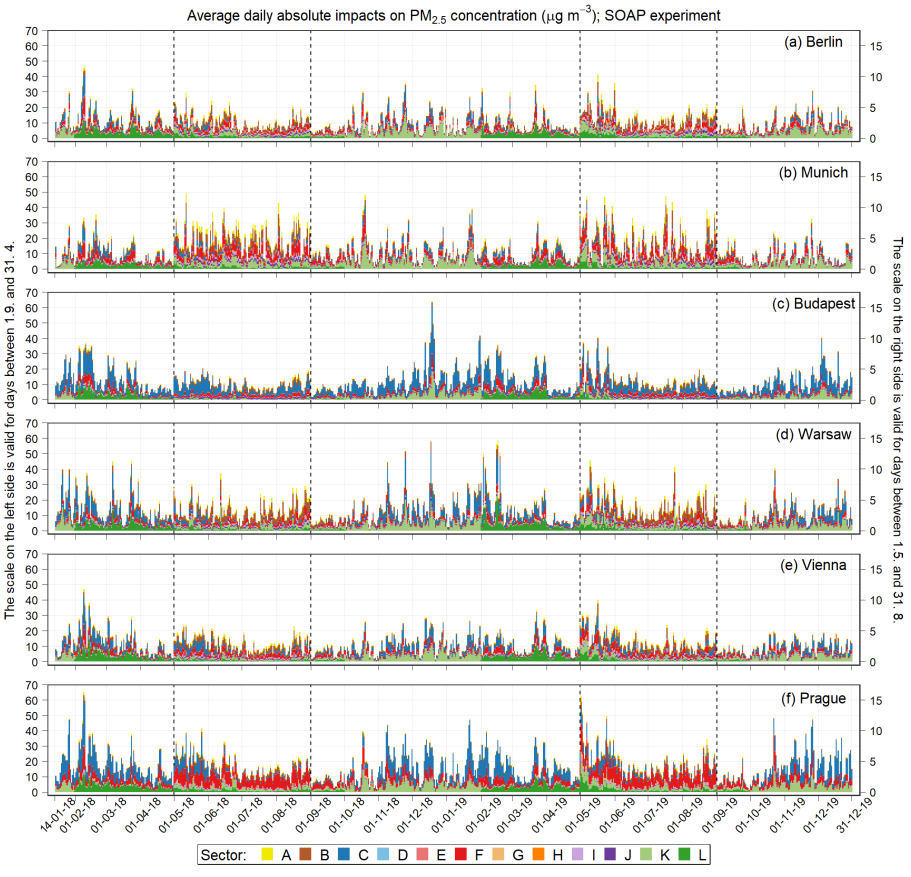

Figure 20. Temporal evolution of the average daily absolute impacts of emissions from individual GNFR sectors A–L on the concentration of $PM_{2.5}$ (in $\mu g m^{-3}$) above Berlin **(a)**, Munich **(b)**, Budapest **(c)**, Warsaw **(d)**, Vienna **(e)**, and Prague **(f)** in the SOAP experiment. The scale on the left (right) side is valid for the days between 1.9. and 31.4. (1.5. and 31.8.).

https://doi.org/10.5194/egusphere-2023-1919
Preprint. Discussion started: 12 September 2023
© Author(s) 2023. CC BY 4.0 License.

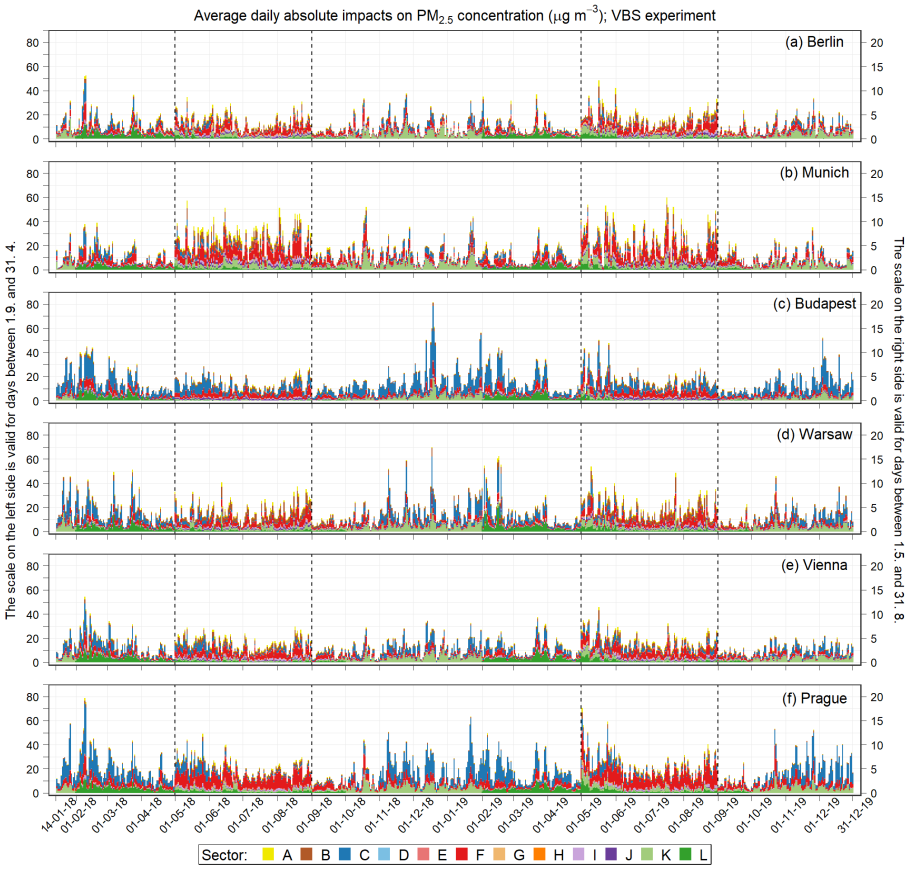

Figure 21. Same as Fig. 20 but for the VBS experiment.

https://doi.org/10.5194/egusphere-2023-1919
Preprint. Discussion started: 12 September 2023
© Author(s) 2023. CC BY 4.0 License.

Table 1. Overview of GNFR sectors used in the study.

Sector	Sector name
A	Power plants
B	Industrial sources
C	Other stationary combustion
D	Fugitives
E	Solvents
F	Road transport
G	Shipping
H	Aviation
I	Off-road
J	Waste
K	Agriculture–livestock
L	Agriculture–other

Table 2. List of model experiments performed.

Experiment	Number of simulations	OA mechanism	PSAT applied
SOAP	13*	SOAP	No
VBS	13*	1.5-D VBS	No
PSAT	1	SOAP	Yes

* One base simulation (in which emissions from all sources were considered) + 12 perturbed simulations (in each of them, emissions from one of the GNFR sectors A–L were set to zero).

https://doi.org/10.5194/egusphere-2023-1919
Preprint. Discussion started: 12 September 2023
© Author(s) 2023. CC BY 4.0 License.

Table 3. Comparison of modeled (the base simulation of the SOAP/VBS experiment and the simulation of the PSAT experiment) and measured (AirBase data) daily concentrations of $PM_{2.5}$ in 2018–2019 at suburban and urban stations in Berlin, Munich, Budapest, Prague, and Vienna: evaluation of the Pearson correlation coefficient (r), normalized mean bias (NMB, in %), and normalized mean square error (NMSE, in %) averaged over all stations in each city. DJF, MAM, JJA, and SON refer to the winter (covering December–January–February), spring (March–April–May), summer (June–July–August), and autumn (September–October–November) seasons, respectively.

City	$PM_{2.5}$	r			NMB (%)			NMSE (%)		
		SOAP	VBS	PSAT	SOAP	VBS	PSAT	SOAP	VBS	PSAT
Berlin	DJF	0.81	0.82	0.81	-32.3	-26.1	-32.3	45.4	33.9	45.3
	MAM	0.56	0.59	0.56	-51.4	-45.6	-51.1	102.7	79.8	101.6
	JJA	0.55	0.62	0.55	-75.8	-68.0	-75.6	274.3	169.42	270.7
	SON	0.70	0.73	0.71	-48.6	-41.0	-48.4	84.0	59.6	83.2
Munich	DJF	0.79	0.80	0.79	1.5	13.7	1.6	22.6	21.9	22.6
	MAM	0.73	0.73	0.73	-33.1	-23.4	-32.8	66.4	48.6	65.7
	JJA	0.48	0.51	0.48	-48.2	-35.1	-47.6	70.4	39.5	68.4
	SON	0.72	0.73	0.72	-14.1	-0.4	-13.7	23.7	19.2	23.4
Budapest	DJF	0.66	0.68	0.66	-19.5	-3.0	-19.5	32.0	23.1	31.9
	MAM	0.43	0.45	0.43	-40.8	-30.7	-40.5	68.2	54.3	67.4
	JJA	0.38	0.36	0.39	-72.1	-63.9	-71.9	219.4	139.1	217.1
	SON	0.63	0.63	0.63	-50.7	-40.3	-50.4	88.4	56.0	87.3
Prague	DJF	0.74	0.75	0.74	5.4	19.7	5.4	28.0	28.5	28.0
	MAM	0.58	0.59	0.58	-27.5	-19.6	-27.2	44.9	37.4	44.4
	JJA	0.38	0.41	0.38	-64.3	-57.3	-64.0	147.7	102.9	145.1
	SON	0.51	0.51	0.51	-26.0	-18.3	-25.7	59.8	53.0	59.4
Vienna	DJF	0.65	0.67	0.65	-29.4	-22.2	-29.4	49.7	38.0	49.6
	MAM	0.73	0.74	0.74	-43.3	-36.1	-42.9	73.3	53.9	72.7
	JJA	0.33	0.28	0.33	-63.4	-52.9	-63.0	138.6	84.0	135.6
	SON	0.55	0.56	0.56	-49.2	-41.6	-48.9	117.4	88.8	115.9